DEVELOPMENT OF INTERIOR BALLISTIC SIMULATION SOFTWARE

A THESIS SUBMITTED TO
THE GRADUATE SCHOOL OF NATURAL AND APPLIED SCIENCES
OF
MIDDLE EAST TECHNICAL UNIVERSITY

BY

FAİK DANIŞ

IN PARTIAL FULFILLMENT OF THE REQUIREMENTS
FOR
THE DEGREE OF MASTER OF SCIENCE
IN
MECHANICAL ENGINEERING

FEBRUARY 2014

Approval of the thesis:

DEVELOPMENT OF INTERIOR BALLISTIC SIMULATION SOFTWARE

submitted by **FAİK DANIŞ** in partial fulfillment of the requirements for the degree of **Master of Science in Mechanical Engineering Department, Middle East Technical University** by,

Prof. Dr. Canan ÖZGEN
Dean, Graduate School of **Natural and Applied Sciences** _____

Prof. Dr. Süha ORAL
Head of Department, **Mechanical Engineering** _____

Prof. Dr. M. Haluk AKSEL
Supervisor, **Mechanical Engineering Dept., METU** _____

Dr. Mehmet Ali AK
Co-Supervisor, **ROKETSAN** _____

Examining Committee Members:

Prof. Dr. Kahraman ALBAYRAK
Mechanical Engineering Dept., METU _____

Prof. Dr. M. Haluk AKSEL
Mechanical Engineering Dept., METU _____

Dr. Mehmet Ali AK
ROKETSAN _____

Prof. Dr. Abdullah ULAŞ
Mechanical Engineering Dept., METU _____

Assoc. Prof. M. Metin YAVUZ
Mechanical Engineering Dept., METU _____

Date: **11/02/2014**

I hereby declare that all information in this document has been obtained and presented in accordance with academic rules and ethical conduct. I also declare that, as required by these rules and conduct, I have fully cited and referenced all material and results that are not original to this work.

Name, Surnarme: FAİK DANIŞ

Signature :

ABSTRACT

DEVELOPMENT OF INTERIOR BALLISTIC SIMULATION SOFTWARE

Danış, Faik
M.S. Department of Mechanical Engineering
Supervisor: Prof. Dr. M. Haluk AKSEL
Co-Supervisor: Dr. M. Ali AK

February 2014, 77 pages

In this study, an interior ballistic simulation program is constructed for solid propellant conventional guns. In accordance with this purpose, interior ballistic calculations are studied numerically and two numerical models are produced: zero dimensional model and one dimensional model. Zero dimensional model, which is based on lumped parameter approach, examines variation of ballistic parameters with ignition of propellant grains in order to find muzzle velocity. In one dimensional code, the problem is modeled as one dimensionally as inviscid flow and Roe approximate Riemann solver is used as solution technique. Both of the models can simulate real gas flow by introducing covolume based on Noble-Abel equation of state. The differences between numerical models are examined.

Keywords: Interior Ballistics, Lumped Parameter, Covolume, Real Gas, Inviscid Flow, One Dimensional Flow, Roe Riemann Solver

ÖZ

İÇ BALİSTİK SİMÜLASYON YAZILIMI GELİŞTİRİLMESİ

Danış, Faik
Yüksek Lisans, Makine Mühendisliği Bölümü
Tez yöneticisi: Prof. Dr. M. Haluk AKSEL
Ortak Tez yöneticisi: Dr. M. Ali AK

February 2014, 77 sayfa

Bu çalışmada, katı yakıtlı geleneksel silahlar için bir iç balistik simülasyon programı oluşturuldu. Bu amaçla, iç balistik hesaplamaları nümerik olarak çalışıldı ve iki numeric model oluşturuldu; sıfır boyutlu model ve bir boyutlu model model ortaya konuldu. Yığılı parametre yaklaşımına dayanan sıfır boyutlu modelde barut taneciklerinin ateşlenmesiyle birlikte balistik parametrelerin değişimi incelendi. Bir boyutlu kodda, problem bir boyutlu viskoz olmayan akış olarak modellendi ve Roe yaklaşık Riemann methodu çözüm tekniği olarak kullanıldı. Her iki kodda gerçek gaz akışını simüle etmesi için Noble-Abel hal denklemindeki gibi eş hacim tanımlandı. Her iki numerik kod arasındaki farklar incelendi.

Anahtar kelimeler: İç Balistik, Yığılı Parametre, Eş Hacim, Gerçek Gaz, Viskoz Olmayan Akış, Bir Boyutlu Akış, Roe Riemann çözücüsü

To my family

ACKNOWLEDGEMENTS

I would like to express my sincere gratitude to my supervisor Prof. Dr. Mehmet Haluk AKSEL and my co-supervisor Dr. Mehmet Ali AK for his helpful guidance, motivation and understanding in the progress of this study.

I would also like to express my sincere appreciation to Dr. Cevat Şener for his support in building graphical user interface.

This study was supported through SAN-TEZ program by Republic of Turkey Ministry of Science, Industry and Technology.

TABLE OF CONTENTS

LIST OF TABLES

TABLES

LIST OF FIGURES

FIGURES

LIST OF SYMBOLS

a	Acceleration speed of sound
A	Area, Jacobian matrix
b	Covolume
B	Burn Rate Coefficient
C_P	Specific Heat at Constant Pressure
C_v	Specific Heat at Constant Volume
D	Diameter
e	Specific Internal Energy
E	Energy
F	Impetus, Flux Vector
I	Inertia
L	Length
m	Mass
n	Burn Rate index, Number of Propellant types, Number of cells
N	Total Number of Propellants
Q	Total Energy
p	Pressure
R	Specific Gas Constant
r_d	Regression distance
S	Distance, Source term
t	Time
T	Temperature, time
T_0	Flame Temperature
u	Gas Velocity
U	Internal Energy, Conserved Variable Vector
V	Velocity
W	Work

Z	Fraction of Propellant Burnt, Form Factor
γ	Specific Heat Ratio
κ	Pidduck-Kent Constant
ξ	Heat Loss Coefficient
θ	Twist Angle
v	Specific Volume
ρ	Density
$\forall$	Volume
Φ	Correction Factor

Subscripts

0	Initial
ave	Average
c	Charge
bore	Barrel Bore
eff	Effective
i	Inner
o	Outer
ig	Igniter
p	Projectile
r	Resistance
rband	Rotating Band

CHAPTER 1

INTRODUCTION

1.1 Literature Review

Interior ballistics of conventional guns is the study of conversion of chemical energy of solid propellants into the kinetic energy of a projectile. It can be described as a piston-cylinder problem in which the piston is thrown away with the force produced by the combustion of gun powder in closed cylinder volume. The main concern of interior ballistics is the phenomena going over the period between the ignition of propellant and the leaving of projectile from barrel tube. The aim of gun interior ballistics is to predict the temperature, pressure, velocity and density history of gases at the base of the gun and projectile at all times during the firing.

Interior ballistics wasn't differentiated from exterior ballistics because there was no way of measuring pressure and velocity until the first study of Robins with ballistic pendulum to measure velocity in 1740 in history [1]. Then, Lagrange in 1793 was the first one tried to model interior ballistics by the idea based on the gas density is uniform behind projectile (i.e. it is independent of x) so that the velocity of gas at any instant increases linearly with distance along the bore. The idea is true for the propellant of that time (i.e. black powder) which becomes gas quickly and has less energy content [2]. The problem of releasing a projectile from a hypothetical gun which is initially pressurized and has no friction through barrel tube is known as "Lagrange's Gun" in literature of interior ballistics. In addition, there were contributions made by Vallier, Heydenreich and Leduc. Leduc fitted a hyperbolic curve to experimental data and generate ballistic tables. The practical approach was to solve the problem experimentally at that time. Ballistic parameters assumed by

using observed velocities and peak pressures from empirical treatments were used to predict pressure-space history. In 1860, Resal successfully expressed the underlying equation for energy conversion. There is no reliable theoretical model to solve the gun problem until Charbonnier in 1908. Since there was no information about pressure in the gun due to lack of piezoelectric gauges in 1935, numerous simplifications were made to setup the analytical model [1].

There were great contributions made by Love and Pidduck (1922) and the gun problem which is commonly called "Lagrange's Ballistic Problem" was solved analytically [3]. This study was then improved by Kent in 1936 and Vinti and Krawitz in 1949. Various simplifications were made to solve the gun problem. Firstly, the chamber is replaced by a volumetrically equivalent barrel tube having the same diameter. Secondly, the charge is considered to be in gaseous form (i.e. all solid propellant is burnt instantaneously in the combustion chamber). Thirdly, there are no primary energy loses like heat loss, frictional loss, gas leakages etc. Pidduck-Kent model addresses the non-uniformity of gas, which is important for high charge to projectile mass ratio. In these studies, although the flow was studied as expansion of gaseous combustion products with the assumptions stated previously, there were still relatively complex problems of tracing rarefaction waves produced by motion of projectile in order to reach an analytical solution.

In earlier times of studies of interior ballistics, the ballistic problem was simulated by curve fittings on experimental data or by using closed form solutions obtained from analytical solutions and tabulating the data from the closed form solutions. Roogle, Bennet, Hirschfelder [4] developed useful tables providing performance estimates based on grain dimensions, charge mass etc. These tables are still used by today's balisticians. A breakthrough has happened with the invention of digital computers. By the help of a digital computer, the ballisticians started to consider theoretical solutions by eliminating simplifications to a degree. These approaches, which have a great deal of mathematical complexity, require the substitution of the best available values for parameters to form a numerical program.

Baer and Frankle introduced the first numerical solution to differential equations in interior ballistics in 1960's with various assumptions to model the problem [5]. Different from Lagrange's approach, which simulates the burning of propellant as instantaneous and model the flow behind the moving projectile as expansion of gaseous products, the code done by Baer and Frankle is taking into account the volume of solid propellant grains and finite rate burning of propellant charge and it is based on lumped parameter approach. Another most notable study which was called NOVA, was carried out by Stiefel [6]. These codes were unable to analyze the structure of pressure field and the longitudinal rarefaction waves created by the motion of projectile and its reflection from the walls of gun. Therefore, the effect of these problems is embedded into code by introducing correction factors.

Interior Ballistics of High Velocity Guns Version 2 (IBHVG2) code has been one of the most widely used interior ballistic model based on Baer-Frankle's studies [7]. It is a lumped parameter model. Projectile Design and Simulation Program (PRODAS) is a commercial program that can simulate both interior and exterior ballistics. PRODAS uses IBHVG2 code to model gun interior ballistics [8]. This model has a high degree of reliability when the results of model are compared with experimental data although it uses various correction factors.

A constant pressure code (CONPRESS) of interior ballistics, which assumes that the combustion of propellant and motion of the projectile takes place under a constant pressure to find conditions at muzzle, is also a lumped parameter code. It is commonly used for the estimation of propellant performance [9].

Gough [10] developed XNOVAKTC code which models the interior ballistic problem as one dimensional two phase flow consisting of condensed propellant and combustion gases. Two phase flow becomes important when designing ammunition where the primer and propellant interface of propellant charge is important. Two phase flow has been a developing topic reaching today. Another study made in 2005 is also based on solving interior ballistic problem as one-dimensionally with two

phase flow and non-conservative scheme [11]. An axisymmetric model is done to examine interior ballistic performance of projectiles using granular or tubular type solid propellants [12]. Ignition of solid propellants and the phenomenon of flame spreading is studied by Lowe in 1996 [13].

A three dimensional, two phase numerical simulation of interior ballistic of mortar systems can also be done [14]. The fundamental aim of the latter studies should be to construct a gun propulsion program that is modular and can handle traditional solid propellants designs, regenerative liquid propellants design and various electrothermal-chemical designs [15].Next Generation Code (NGEN) is developed by Paul Gough and improved by Nusca and Horst [4,15]. NGEN is a multiphase, three dimensional code using Eulerian-Lagrangian approach, which can handle telescoped ammunition configurations which require handling of flame spreading or can handle guns with different projectile configurations like mortar tube. NGEN can handle regenative liquid propellants and various electrothermal-chemical weapons. NGEN has been studied since 1990s in order to construct a single, modular program that can solve interior ballistics of different gun-projectile configurations. is a modular program to solve gun interior ballistic problem.

1.2 Scope of Thesis

Today, there are various of gun and ammunition configurations so that it is a very complex process to make an interior ballistic program which is valid for all of them since there are various concepts for different propulsion systems. In addition, every gun interior ballistic problem is based on a number of simplifying assumptions to reduce the problem to an analyzable form. It is much better to use separate codes with various level of difficulties for different gun systems. This thesis is aimed to simulate the interior ballistics of conventional arms to improve their design. A lumped parameter code and one dimensional code were done to achieve this goal.

1.3 Outline of Thesis

In Chapter 2, the information about basic definitions of gun interior ballistics and general criteria about gun design is improved. In Chapter 3, zero dimensional model (i.e lumped parameter code) is explained in detail. In Chapter 4, information about one dimensional code is presented. In Chapter 5, zero and one dimensional code models are verified by using the data available in literature.

CHAPTER 2

BACKGROUND ON GUN DESIGN

In this chapter, the basic terminology about arms and the important parameters in designing a gun are given for better understanding of the interior ballistic concepts. In addition, the events occurring while firing a ammunition, which is also called a "ballistic cycle", are explained.

2.1 Gun Nomenclature and Design

Barrel bore is the internal part of the barrel with a tapered opening at the breech to house the cartridge. The typical gun barrel bore consists of four parts: breech, cartridge chamber, forcing cone and riffled barrel tube [16]. In Figure 2.1, the main parts of barrel bore are illustrated. The breech is the rear part of barrel where the mechanism feeding the cartridge into gun places. Breech block is designed to resist high stress and temperature because it prevents the gas leakage from combustion of propellant to protect the gunner. The cartridge chamber serves to house the ammunition in the barrel. It is the place where the combustion of propellant charge occurs.

The cartridge case seals the rear end of the barrel for preventing gas leakage. It has a conical shape with clearance. It is designed for easing the loading and ejecting the case after firing. In Figure 2.2, a close view of cartridge in combustion chamber can be seen. However, the shape of cartridges is not unique in literature. There are various types of cartridge cases for different type of guns in military stocks such as rimes head, rimless head, bottleneck shape, tapered shaped or straight shaped cartridges.

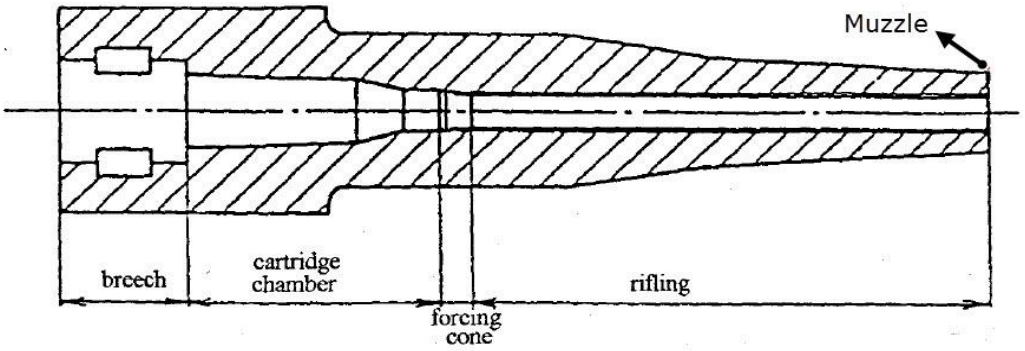

Figure 2.1: Main parts of barrel bore[16]

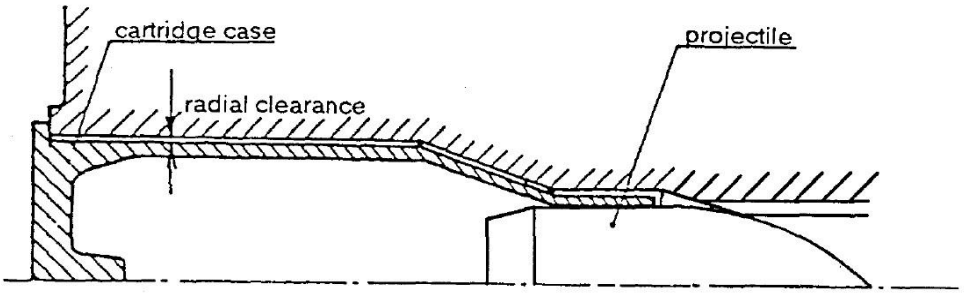

Figure 2.2 : The schematic view of the cartridge case in the combustion chamber[16]

Forcing cone is used to support the projectile at the start of ignition and also ensure sealing. Riffling part of barrel bore is the place where the acceleration of projectile takes place. Riffling is a set of twisted grooves cut along the interior of the bore, leaving lands between them. The projectile, is commonly called bullet, is fitted inside cartridge having a soft metal rotating band near its base. The main aim of designing projectile with a rotating band is to assist projectile moving along the longitudinal axis of bore and increase the aerodynamic stability of the projectile when leaving the muzzle. This is achieved by imparting spin into projectile when the bullet is imparted with the rifling of the bore. In addition, rotating band acts a safety belt for gas leakage ahead of the projectile. Furthermore, it provides the initial pressure rise by introducing an initial resistance to movement which is important for the regularity of burning of propellant charge.

In Figure 2.3, a cross-sectional view of riffled barrel bore can be seen. In Figure 3, D_G is the diameter of grooves, D_L is the diameter of lands, W_G is the width of grooves and W_L is the width of lands. Riffling can be imparted in barrel bore as trapezoidal or circular instead of rectangular shape. In addition, the shape of barrel riffling profile can be constant angle helical, varying angle helical, cubical or parabolic type. Constant angle helical riffling profile is commonly used in most of the guns. The others are used for special cases where it is needed to change the pressure curve by riffling [17]. The pitch of riffling is the distance needed for a full turn of projectile. The pitch of riffling or twist angle or riffling is also a design criterion affecting the muzzle velocity. The front part of barrel bore is called muzzle. Muzzle velocity which is the velocity of the projectile, when it leaves the gun bore. It is a desired output parameter for interior ballistics since it will be used when analysing the exterior ballistics of a projectile.

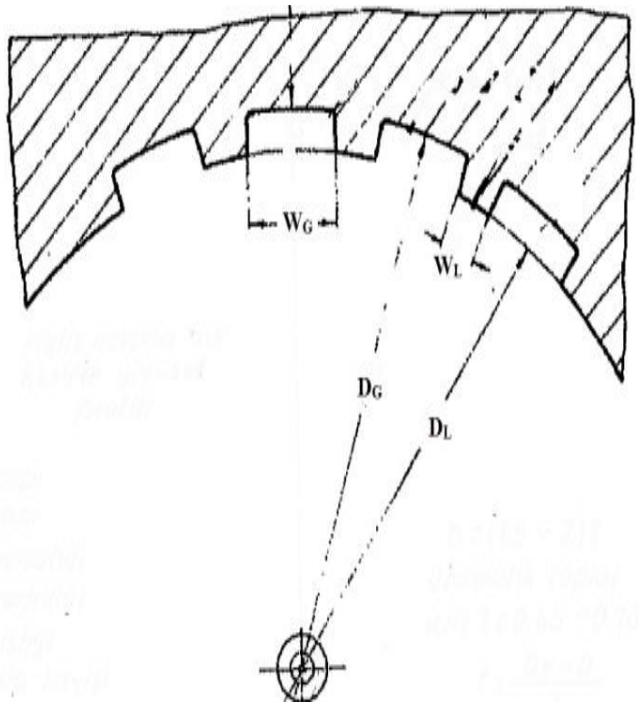

Figure 2.3 : Cross-sectional view of barrel tube [17]

The cartridge and barrels are expressed in terms of bore diameter. Caliber is the diameter of the bore, excluding the depth of riffling grooves. It is measured from land to land. It is widely used in military area. For example, 7.62x51 mm cartridge means that the diameter of cartridge is 7.62 mm and the length or cartridge case is 51 mm. However, it is commonly called caliber of 7.62 when talking about the cartridge in daily use. In addition, in British unit systems, caliber is expressed in inches and it is referred by excluding the decimal point in common language for small arms. For example, 7.62 mm caliber which is equal to 0.30 inches is referred to as thirty calibers in British unit sources. In addition, a 7.62x20 mm caliber barrel tube indicates that the diameter of barrel tube is 7.62 mm and the length of barrel tube is twenty times the diameter of the gun bore.

A small amount of primer propellant which is composed of sensitive chemical material to impact is used to increase the temperature of the cartridge in order to burn the main propellant charge efficiently. It is also called igniter propellant. The needle in breach mechanism strikes the base of cartridge and the primer explodes instantaneously. By the help of the flame channels, the heat passes into main propellant [16]. In Figure 2.4, a schematic view of a cartridge parts can be seen.

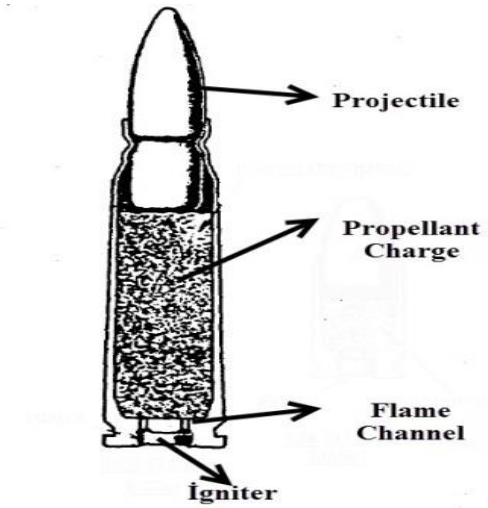

Figure 2.4 : Main parts of a cartridge[16]

Projectiles are designed for minimum drag and maximum impact on target and stability in the air. To reduce the drag force at supersonic velocities, the tip of the projectile is made highly tapered. It is also tapered but in a less degree at the rear part in order to reduce drag for subsonic flows. Rotating bands is made for air stabilization as stated previously. However, there are projectiles without rotating band and having a diameter slightly larger than the diameter of barrel bore. They are also called body-engraved projectiles and are in common use in small arms. Air stabilization can be imparted to projectile by attaching boom and fins in projectile if desired. Projectile can be designed to increase destructive effect on target by imparting high strength material. The material of other parts of projectile is also important when the mass of projectile and engraving frictional force that have a role on the pressure behind projectile are considered [18]. In Figure 2.5, the terminologies about projectile can be seen.

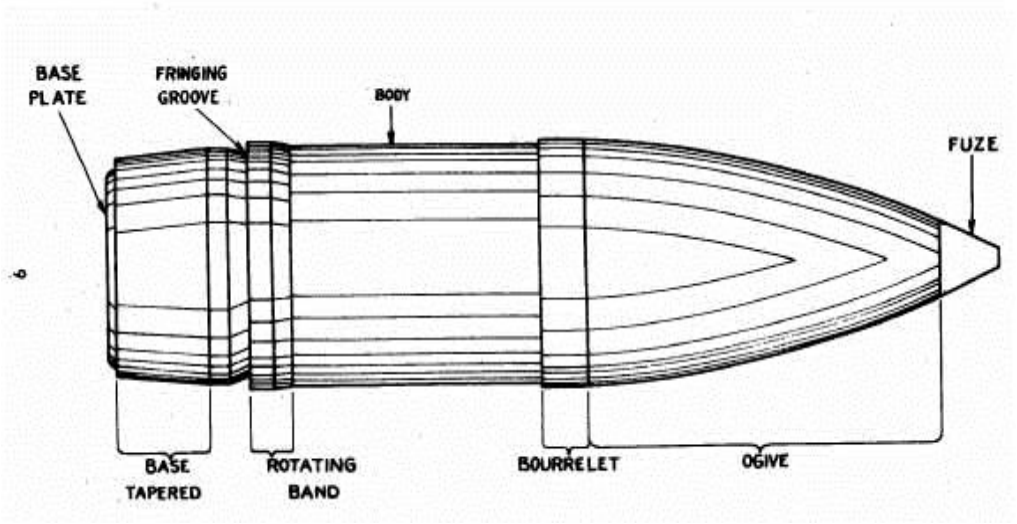

Figure 2.5 : Typical projectile terminology [19]

2.2 Propellant Grain Design

In interior ballistics of gun, the chemical energy of propellant is transformed into kinetic energy of projectile. Thus, the choice of propellant grains producing the propulsive force to move projectile is an extremely important issue. Propellant charges chemically contain the oxygen needed to burn; so, there is no need for systems to take oxygen to combustion chamber. However, there is also less content of oxygen in propellant in order to prevent instinctively burning. Therefore, there occur unburned gases in barrel and if they meet the atmosphere, they continue to burn and forms the phenomena of muzzle flame [20].

Most of the today's propellants are smokeless and are extremely powerful when compared to black powder of old times. They can be single, double, or triple based propellant having different chemical composition. Single based propellants have less sensitivity and the burning of propellant can be controlled easily with additives. Double-based propellants have higher sensitivity and burning rate higher than single-based ones but it can still be controlled. However, manufacturing of propellant isn't safe as single ones due to nitroglycerin and erodes bore due to existing of higher temperatures. Triple based propellants can burn at low temperatures and have low erosion potential but they still have high propulsion.

Other than chemical composition, the burn rate of propellant is also strictly dependent on the pressure acting on the surface of grain where combustion gases emerge. Mass generation of combustion gases is dependent on burn rate of propellant. In addition to regression rate, mass generation of combustion gases is also also related to surface area of propellant exposed to burning. Therefore, the selection of appropriate grain configurations is also important in interior ballistics. There are various shapes of gun propellant like ball, cord, single perforated, seven perforated, rosette etc. In Figure 2.6, the types of grains can be seen. Perforation of propellant grain is used as a way to increase formation of gas by increasing the surface area [20]. Ball, cord or single perforated propellant grains are used for small arms.

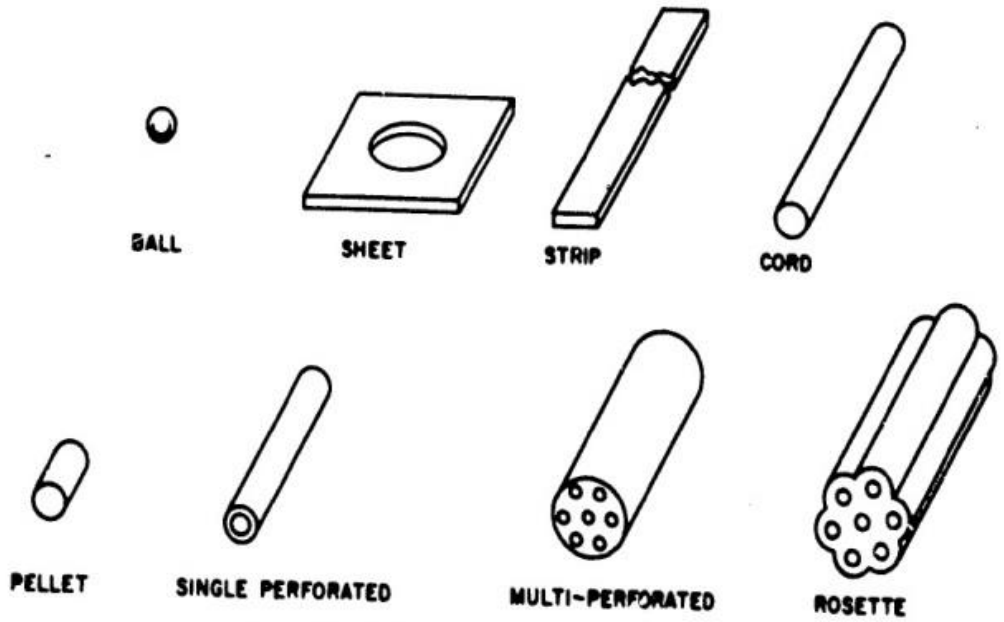

Figure 2.6 : Type of propellant grains[20]

The change in area of propellant grains during burning isn't the same for all types of grains. In addition, propellant grains are classified as neutral, regressive or progressive type according to burning actions. In Figure 2.7, the effect of grain shapes on surface area with respect to percent of burnt mass of propellant can be seen. Cord and strip forms are regressive type of propellants because the total surface area of propellant grain per unit weight decreases while burning. Single perforated grains are of neutral type because the total surface area doesn't change during burning. The increase in inner surface of the grain is equal to the decrease in outer surface of grain if large length to thickness ratio is chosen. Multi-perforated and rosette type grains are progressive type propellant grains because the total surface of area is increasing while burning. However, multi-perforated grains aren't fully consumed since there is an irregular formation of sliver due to unburned grains. For this reason, irregular muzzle velocities can be obtained [20]. By changing the size of grains, progressive or regressive character of propellant grains can be altered for the same type of grain. For example, by lowering the length to thickness ratio, grains of neutral type can be obtained [19].

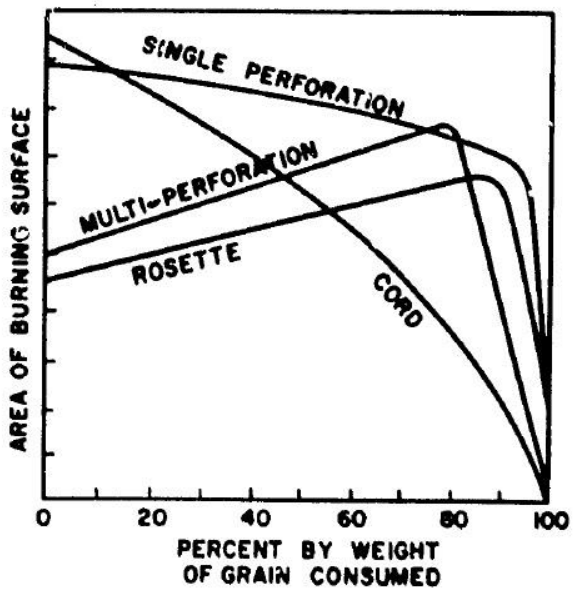

Figure 2.7 : The change in surface area per unit weight for different granulations [20]

The character of grain configuration has an important role on gun performance by changing the sensitivity of pressure versus travel curve. In Figure 2.8, these properties are illustrated. If the charge weight is kept constant and grain size is increased lower pressures with higher muzzle pressures can be obtained and there is higher possibility of emerging blast at muzzle due to pressure difference with environment. Also, the repulsion of gun will be higher. If the charge configuration is changed to a progressive one while keeping the initial surface and charge weight of grain same, lower peak pressures can be obtained. Furthermore, if the grain size and configuration are kept the same, there will be lower peak pressures for lower charge weight [19].

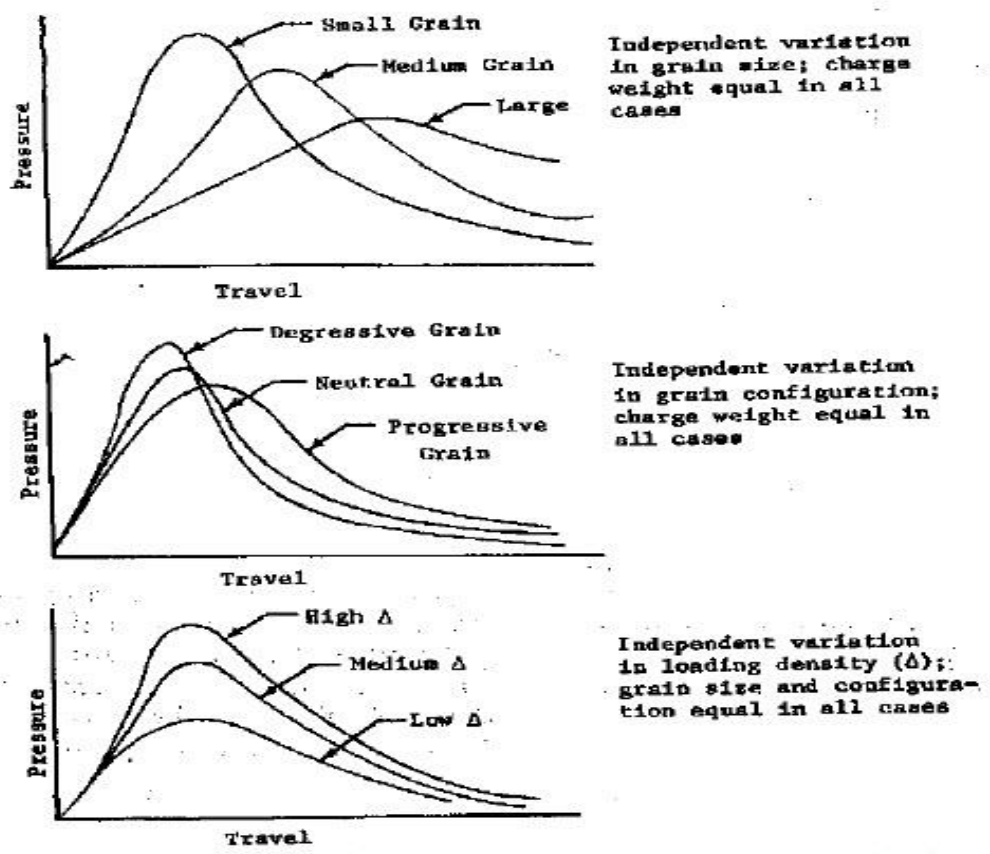

Figure 2.8 : Sensitivity of pressure versus travel curve to grain configurations [19]

2.3 Interior Ballistic Cycle

All the events occurring in every firing of gun between the ignition of propellant and the leaving of projectile is called interior ballistic cycle. Interior ballistic cycle can be summarized as in the following [16]:

a) The striker hits the cartridge cap.
b) There is a delay before ignition sequence starts. The primer propellant detonates to produce a flame which ignites the outer surface of propellant
c) Pressure rises inside the cartridge case until it is sufficient to blow the bullet out of the mouth of cartridge. Considerable resistance is encountered as the bullet is engraved in the riffling.
d) The propellant produces combustion gases faster than the increase in the volume behind the projectile; therefore, the pressure rises rapidly

e) At this point the highest pressure is obtained.

f) The velocity of bullet is now so great that the increase in volume behind the projectile is growing faster than the propellant can fill it and so pressure starts to drop.

g) The propellant is all burnt.

h) The bore behind the bullet remains full of hot gas that expands adiabatically.

i) The bullet emerges from the muzzle, and some of gases overtake it. Pressure in the gun bore remains relatively high. Although the bullet is moving in the gun bore for few milliseconds, it may reach a velocity up to 1000 m/s at the muzzle and the maximum acceleration is approximately $1.5x10^6$ m/s^2.

j) For a further 2 or 3 ms, pressure continues to drop in the bore. At this stage, it is safe to unlock the feeding mechanism to take advantage of remaining gas pressure.

k) The pressure in the bore drops to ambient pressure.

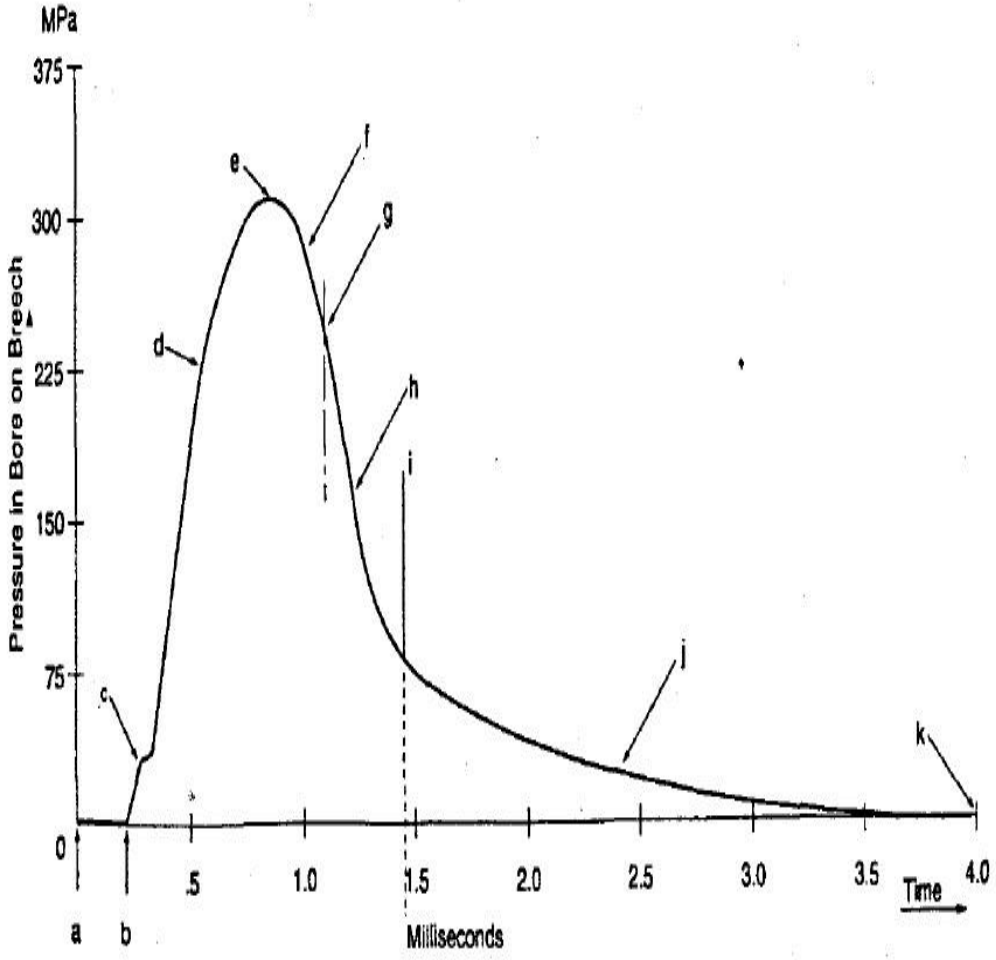

Figure 2.9 : Pressure – time curve for ballistic cycle [16]

CHAPTER 3

ZERO DIMENSIONAL MODEL

Zero dimensional model, which is based on lumped parameter approach and used to predict the performance of guns, will be introduced in this chapter. In this model, solid propellant grains are assumed to be burnt at the space-averaged temperature in the variable volume behind the projectile. Time wise variation of all parameters is calculated upon the ignition of propellant. A pressure gradient model is used as correction to express the real pressure acting on the base of the projectile. The volume of solid propellant grains are taken into account as in the real cases. Different propellant granulations with more than one propellant in the chamber can be modeled. Linear finite rate burning of propellant is modeled similar to the real cases. Flame spreading is ignored. The chamber volume is assumed to have the same diameter with barrel bore. It is assumed that the propellants have uniform distribution in the chamber and all propellant grains recess by the same amount in time. All the losses are expressed by using correction factors.

Zero dimensional model is commonly preferred since it is simple and requires less computation time in computing gun performance calculations. The solution algorithm is based on the numerical integration of ordinary differential equations. Equation of energy, equation of state, equation of pressure gradient, equation of motion and equation of burning are solved successively to predict gun performance. References [5], [7] and [19] are highly used to constitute this model.

3.1 Equation of Energy

Zero dimensional model is primarily based on the time integral of conservation laws from 0 to t to calculate ballistic parameters and can be seen in the following equation.

$$\int_0^t \frac{\mathrm{d}}{\mathrm{d}t} \int_{CV} U \ \mathrm{d}\forall \, \mathrm{d}t + \int_0^t \int_{CS} F \bullet n \ \mathrm{dA} \, \mathrm{d}t = 0$$

In interior ballistics, the energy, which gives motion to the bullet, is released by the combustion of propellant. The total energy of the system primarily depends on the sum of energy of gases produced due to combustion of each propellant having different chemical compositions. In parallel to energy, the same approach can be used in the calculation of the total gas pressure emerged from burning of solid propellant grains. According to first law of thermodynamics, the difference between the chemical energy of solid propellant grains which will be burned gradually, Q and work done while moving the projectile, W is equal to the sum of internal energy of burned gases in chamber volume and energy loses in the system emerged from heat transfer. These relations can be seen in equation (3.1) and (3.2).

$$Q - W = U + E_{losses} \tag{3.1}$$

$$Q = \sum_{i=1}^{n} \left(m_{c_i} Z_i \int_0^{T_{0_i}} c_{v_i} \mathrm{d}T \right) \tag{3.2}$$

In these formulations, n represents the total number of propellant types, m_c is the mass of propellant charge, Z_i is the fraction of volume of burned propellant to initial volume of solid propellant charge at a time, T_0 is the adiabatic flame temperature of propellant charge and c_v is the constant volume specific heat capacity for propellant charge. In addition, it should be noted that the expression $m_c Z$ at a specific time

represents the amount of mass of the solid propellant burnt and transformed into combustion gas.

In order to represent the character of how fast the grain produces gas from its surface for different configurations, form factors Z are used. Form factors are purely geometrical relations which are used to express the mass of the propellant burnt at any time. Cubic form relations in burning surface regression distance are derived by Stals for different type of charges with inhibited or uninhibited surfaces and sliver burn [21]. Form factors and the relations showing the change of surface area and volume with regression distance can be seen in Table 3.1. It should be mentioned that regression distance, r_d, is zero before ignition and increasing with time while burning. In Table 3.1, A_0, A, $\forall_0$ and $\forall$ represents the initial surface area of propellant grain, the surface area of propellant grain at t, the initial volume of propellant grain and the volume of grain at t, respectively.

Because of the expansion of gas and work done on projectile, it is expected that the temperature of burned gases behind the projectile should be lower than propellant's flame temperature. Hence, the internal energy of burned gases is represented as:

$$U = \sum_{i=1}^{n} \left(m_{c_i} Z_i \int_0^T c_{v_i} \mathrm{d}T \right) \tag{3.3}$$

The work done on projectile can be given as:

$$W = A_{bore} \int_0^x p_{net} \, \mathrm{d}x \tag{3.4}$$

where A_{bore} is the effective area gun barrel and p_{net} is the net pressure acting on the base of the projectile. It should be noted that there is static pressure acting on the base of bullet because of movement of the projectile.

Table 3.1: Form factors and the relations of surface area and volume for different type of propellant grains

Ball	$A_0 = \pi D^2$ $A = \pi(\mathrm{D} - 2r_d)^2$ $\forall_0 = \pi D^3 / 6$ $\forall = \pi(\mathrm{D} - 2r_d)^3 / 6$ $Z = 1 - \forall / \forall_0 = \frac{6}{D} r_d - \frac{12}{D^2} r_d^{\,2} + \frac{8}{D^3} r_d^{\,3}$
Chord	$A_0 = \pi D(0.5\,\mathrm{D} + L)$ $A = \pi(\mathrm{D} - 2r_d)^2[0.5(\mathrm{D} - 2r_d) + (\mathrm{L} - 2r_d)]$ $\forall_0 = 0.25\pi D^2 L$ $\forall = 0.25\pi(\mathrm{D} - 2r_d)^2(L - 2r_d)$ $Z = 1 - \forall / \forall_0 = \left(\frac{2(\mathrm{D} + 2\,\mathrm{L})}{DL}\right) r_d - \left(\frac{4(2D + L)}{D^2 L}\right) r_d^{\,2} + \left(\frac{8}{D^2 L}\right) r_d^{\,3}$
Multi Perforated	$A_0 = \pi L(D_o + N D_i) + 0.5\pi(D_o^{\,2} - N D_i^{\,2})$ $A = \pi(L - 2r_d)[(D_o - 2r_d) + N(D_i + 2r_d)] + \ldots$ $\ldots.0.5\pi[(D_o - 2r_d)^2 - N(D_o + 2r_d)^2]$ $\forall_0 = 0.25\pi L(D_o^{\,2} - N D_i^{\,2})$ $\forall = 0.25\pi(L - 2r_d)^2[(D_o - 2r_d)^2 - N(D_i + 2r_d)^2]$ $Z = 1 - \forall / \forall_0 = a_1 r_d - a_2 r_d^{\,2} + a_3 r_d^{\,3}$ $a_1 = \frac{2[2L(D_o + N D_i)^2 + D_o^{\,2} - N D_i^{\,2}]}{L(D_o^{\,2} - N D_i^{\,2})}$ $a_2 = \frac{-4[2(D_o + N D_i) - L(N - 1)]}{L(D_o^{\,2} - N D_i^{\,2})}$ $a_3 = \frac{-8(N - 1)}{L(D_o^{\,2} - N D_i^{\,2})}$

If equations (3.2), (3.3) and (3.4) are substituted into equation (3.1) and are arranged equation (3.5) can be easily gathered [5].

$$\sum_{i=1}^{n}\left(m_{c_i} Z_i \int_{0}^{T_{0i}} c_{v_i} \mathrm{d}T \right) - A_{bore} \int_{0}^{x} p_{net}\, \mathrm{d}x = \sum_{i=1}^{n}\left(m_{c_i} Z_i \int_{0}^{T} c_{v_i} \mathrm{d}T \right) + E_{losses}$$

or

$$\sum_{i=1}^{n}\left(m_{c_i} Z_i \int_{T}^{T_{0i}} c_{v_i} \mathrm{d}T \right) = A_{bore} \int_{0}^{x} p_{net}\, \mathrm{d}x + E_{losses} \tag{3.5}$$

If it is assumed that constant volume specific heat capacity doesn't change considerably from T to T_0, equation (3.5) can be written as:

$$\sum_{i=1}^{n} m_{c_i} Z_i\, c_{v_i} \left(T_{0_i} - T \right) = A_{bore} \int_{0}^{x} p_{net}\, \mathrm{d}x - E_{losses} \tag{3.6}$$

which can be solved for temperature as:

$$T = \frac{\sum_{i=1}^{n} m_{c_i} Z_i\, c_{v_i}\, T_{0i} - A_{bore} \int_{0}^{x} p_{net}\, \mathrm{d}x - E_{losses}}{\sum_{i=1}^{n} m_{c_i} Z_i c_{v_i}} \tag{3.7}$$

At this point, the definition of impetus, which is commonly used as a propellant property in gun interior ballistics, should be made. Impetus, which is also called propellant force, is the energy produced per unit mass of propellant burned and can be given as:

$$F_i = RT_{0i} \tag{3.8}$$

In equation (3.8), F represents impetus and R represents specific gas constant for combustion gas. Specific gas constant is represented in terms of specific heat capacities as:

$$c_p - c_v = R \tag{3.9}$$

with

$$c_v\left(\frac{c_p}{c_v} - 1\right) = c_v\left(\gamma - 1\right) = R \tag{3.10}$$

It is also possible to relate impetus with specific heat ratio as:

$$c_v = \frac{R}{\gamma - 1} = \frac{F}{\left(\gamma - 1\right)T_0} \tag{3.11}$$

If equation (3.11) is substituted into equation (3.7), it is possible to obtain:

$$T = \frac{\sum_{i=1}^{n} \frac{F_i}{(\gamma - 1)} m_{c_i} Z_i - A_{bore} \int_0^x p_{net} \mathrm{d}x - E_{losses}}{\sum_{i=1}^{n} \frac{F_i}{(\gamma - 1)\mathrm{T}_{0i}} m_{c_i} Z_i} \tag{3.12}$$

A small amount of primer propellant having high flame temperature is used as an igniter for the rest of the propellants in chamber volume in gun systems. If igniter propellant is introduced into the above equations, the following equation can be obtained.

$$T = \frac{\sum_{i=1}^{n} \frac{F_i}{(\gamma_i - 1)} m_{c_i} Z_i + \sum_{i=1}^{n} \frac{F_{ig}}{(\gamma_{ig} - 1)} m_{c_{ig}} Z_{ig} - A_{bore} \int_0^x p_{net} \mathrm{d}x - E_{losses}}{\sum_{i=1}^{n} \frac{F_i}{(\gamma - 1)\mathrm{T}_{0i}} m_{c_i} Z_i + \sum_{i=1}^{n} \frac{F_{ig}}{(\gamma_{ig} - 1)\mathrm{T}_{0ig}} m_{c_{ig}} Z_{ig}} \tag{3.13}$$

If the energy losses are excluded explicitly from the work, *W*, needed to move the projectile, then, the work can be taken equal to gain in kinetic energy of the projectile and can be given as:

$$W = A_{bore} \int_{o}^{x} p_{base} \mathrm{d}x = \frac{1}{2} m_p V_p^{\,2} \tag{3.14}$$

In this equation, P_{base} represents the pressure acting at the base of the bullet due to emerging of burned gases, m_p represents the mass of the projectile and V_P represents the velocity of the projectile.

The energy losses in the gun system while the projectile is moving to the muzzle can be gathered into 6 groups:

1. The kinetic energy gained by the burned gasses and unburned solid propellant due to rapid movement of projectile.
2. The heat losses from gun barrel to environment due to non-isolated walls.
3. The energy compensated to overpower frictional forces during motion of projectile.
4. The rotational energy gained due to groove-land configuration.
5. The energy lost due to recoil of gun parts.
6. The strain energy gained by gun during firing

The items 4, 5 and 6 stated above stand for approximately 1-2 % of the total energy. The greatest loss in energy occurs because of residual heat losses of the gases leaving the muzzle, which can be up to 60% percent of the total energy. By the time the projectile leaves the muzzles, it has acquired approximately 30 % of the total energy [18].

Since the projectile is moving so fast, it comes some of the unburned propellant and burned gases with itself. For this reason, the flow behind the projectile should be considered as two phase flow. To compensate this energy losses Pidduck-Kent constant, κ, which is between 3 and 4 should be defined in the problem [7].

$$E_{loss_1} = \frac{1}{2}\frac{\sum_{i=1}^{n} m_{c_i}}{\kappa} V_p^{\,2} \tag{3.15}$$

In another source [19], the effect stated in item 1 is modeled in the system as in (3.16).

$$E_{loss_1} = \frac{1}{2}\frac{\sum_{i=1}^{n} m_{c_i} Z_i}{3} V_p^{\,2} \tag{3.16}$$

It is reasonable to integrate E_{loss1} into the equation of work because the actual weight that should be moved is greater than the weight of projectile as in reality. Therefore, an effective mass should be defined as follows:

$$m_{eff} = m_p + \frac{\sum_{i=1}^{n} m_{c_i}}{\kappa} \tag{3.17}$$

and

$$m_{eff} = m_c + \frac{\sum_{i=1}^{n} m_{c_i} Z_i}{3} \tag{3.18}$$

In addition, the equation of work takes the following form

$$W = \frac{1}{2} m_{eff} V_p^{\,2} \tag{3.19}$$

The heat energy lost from the gun barrel to the environment can be obtained by experimental expression in Reference [22] as :

$$E_{loss_2} = \frac{0.38 D_{bore}^{1.5} \left(L_{muzzle} + \frac{\forall_{c0}}{\mathrm{A}_{bore}} \right) \left(\frac{\sum_{i=1}^{n} m_{c_i} T_{0_i}}{\sum_{i=1}^{c} m_{c_i}} - T_s \right) \mathrm{V}_p^2}{\left(1 + \frac{0.6 D_{bore}^{2.175}}{(\sum_{i=1}^{N} m_{c_i})^{0.8375}} \right) V_p^2} \tag{3.20}$$

In the above equation, D_{bore} represents the diameter of gun barrel, $\forall_{c0}$ represents initial chamber volume and T_s represents the temperature of unburned propellant. U.S units should be used in this equation.

Heat loss from gun tube can also be modeled simply as in the following equation and can directly be substituted in work equation [19].

$$E_{loss_2} = \frac{1}{2} m_{eff} \xi V_p^{\ 2} \tag{3.21}$$

ξ is also an experimental correction factor and it can be taken as 0.17 for medium caliber guns. A higher correction factor should be used for small caliber guns. If ξ can be taken as zero, when there is no heat transfer to the environment in the system [19].

In reference [22], Nordheim defines the heat loss by using convective heat flux. However, a friction factor is also required for expressing the heat transfer coefficient.

After the ignition of propellant, rotating band part of the projectile which has a greater diameter than inner diameter of gun bore should be deformed in order that the projectile can move along the gun barrel. While the width of rotating band is deformed, a very high frictional force occurs compared to the rest of barrel length. This frictional force is also called engraving force. Due to deformation of projectile and sliding frictional force acting along gun tube, there occurs an energy loss.

This loss can be expressed by resistance pressure p_r along the barrel tube and can be given as:

$$E_{loss_3} = A_{bore}\int_0^x p_r \mathrm{d}x = A_{bore}\int_0^t p_r V_p \mathrm{d}t \tag{3.22}$$

In equation (3.22) the integral can be calculated using the trapezoidal rule. Engraving force strictly depends on bore-bullet configuration and how much pressure is required to deform the projectile is unknown. In addition, there is a huge pressure gradient between engraving force and sliding friction force. Therefore, the resistance pressure is defined in the program as a resistance profile which can be changed by the user. There is a resistance profile given in the literature which is obtained by experiments. It can be used by the user as a reference. By using a normalized resistance pressure P_{rn} shown in Table 3.2, resistance profile for different bore-bullet configurations can be obtained [23].

$$p_r = p_{rn}\left(D_{rb} - 1.0\right)\left(w_{rband}\right)\left(FF\right)\left(\frac{1.92}{\left(\frac{w_{groove}}{w_{land}}\right)}\right)\frac{1}{\cos\left(\frac{\theta}{2}\right)} + K_r \tag{3.23}$$

In equation (3.23), D_{rb} represents the diameter of rotating band in calibers, w_{rb} represents the width of rotating band in calibers, FF represents material code, w_{groove} represents width of grooves, w_{land} represents the width of lands, θ represents the angle of lands and K_r is a small residual constant. Material code can be taken as 1 for copper and iron and can be taken 0.2 for plastics, which is stated in Reference [23].

Table 3.2: Normalized resistance pressure profile for projectiles [23]

$P_{rn}(psi)$	P_{rn}(MPa)	Distance (Band Lengths)
2000	13.8	0
15000	103.4	0.2
15000	103.4	0.8
10000	69	1
7000	48.3	1.5
4000	27.6	4
2500	17.2	10
2000	13.8	30
1500	10.3	60
1500	10.3	2000

The rotational energy gained by the projectile can be described as:

$$E_{loss_4} = \frac{1}{2} I_p \omega_p^{\,2} \tag{3.24}$$

In this equation, I_p represents the inertia of the projectile and ω_p represents the angular velocity of the projectile [7]. If the inetia of the projectile isn't known, the following equation can be used.

$$I_p = \frac{1}{8} m_p D_p^{\,2} \tag{3.25}$$

The angular velocity of the projectile can be described with angle of turn (θ_p) at time *t* and the pitch (ϕ) of land configuration which is the distance needed for a full turn of the projectile [7].

$$\theta_p = w_m t \tag{3.26}$$

$$2\pi = \omega_p \left(\frac{D_{bore}\phi}{V_p}\right) \tag{3.27}$$

$$E_{loss_4} = \frac{1}{2}\left(\frac{1}{8} m_p {D_p}^2\right)\left(\frac{2\pi V_p}{D_{bore}}\right)^2 \tag{3.28}$$

There is also a loss due to air drag acting on the front of projectile. The energy to overcome the drag force is quite small so that it can be neglected. However, if necessary it can be taken into account as:

$$E_{loss_{drag}} = F_{drag} A_{bore} = A_{bore} \int_0^x p_{drag} \mathrm{d}x = A_{bore} \int_0^t p_{air} V_p \mathrm{d}t \tag{3.29}$$

If all of the equations stated above is gathered together, the equation required to find the temperature becomes:

$$T = \frac{\sum_{i=1}^{n} \frac{F_i}{(\gamma_i - 1)} m_{c_i} Z_i + \sum_{i=1}^{n} \frac{F_{ig}}{(\gamma_{ig} - 1)} m_{c_{ig}} Z_{ig} - \frac{1}{2} m_{eff} (1+\xi) {V_p}^2 - E_{loss_3} - E_{loss_4} - E_{loss_{drag}}}{\sum_{i=1}^{n} \frac{F_i}{(\gamma_i - 1)\mathrm{T}_{oi}} m_{c_i} Z_i + \sum_{i=1}^{n} \frac{F_{ig}}{(\gamma_{ig} - 1)\mathrm{T}_{0ig}} m_{c_{ig}} Z_{ig}} \tag{3.30}$$

3.2 Equation of State

At the instant of gun firing and during burning of the propellant, the density of emerging gases in chamber volume is increased all of a sudden so that the volume of gas molecules can't be ignored as in the ideal gas law. Otherwise, the margin of error in ballistic model will be quite large for highly energetic propellants or significant loading densities. Therefore, Noble-Abel equation of state, which takes into account of the real behavior of gases should be chosen for modeling interior ballistics. Noble-Abel real gas equation is based on the idea of effective volume that gas molecules can occupy. The difference between specific volume of gases and covolume, b, which shows the degree of volume occupied by gas molecules shows the free volume available for burnt gases that can occupy. Noble-Abel equation of state is very similar to ideal gas law at first look and can be seen in the following equation [7].

$$p_{ave}(v-b) = RT = F\frac{T}{T_0} \tag{3.31}$$

In this equation, P_{ave} represents the average pressure between breechblock and base of the projectile and v represents the specific volume of the burnt gases.

Temperature, T, of burned gases can be found from equation (3.30). In addition, covolume value is specific for each gun propellant and is an input to the ballistic model. If the specific volume of burnt gases, which is increasing with burning of solid propellant grains and is increasing with movement of projectile, is calculated, the average pressure acting on projectile can be found. To calculate the specific volume of burnt gases, it should be remembered that the total mass of burnt gasses at any time *t* is equal to the decrease in the weight of solid propellant until that time.

$$\begin{aligned} p_{ave}\left(\frac{1}{\rho_{gas}} - b\right) &= RT \\ \rho_{gas} &= \frac{m_c Z}{\forall_{gas}} \end{aligned} \tag{3.32}$$

$\forall_{gas}$ is the total volume of the empty space between the base of projectile and breech block.

$$\forall_{gas} = \forall_{c0} + A_{bore}V_p - \frac{m_c}{\rho_c}(1-Z) \tag{3.33}$$

If all of the equations gathered together, average pressure of gases can be given as:

$$\frac{1}{\rho_{gas}} - b = \frac{\forall_{c0} + A_{bore}V_p - \frac{m_c}{\rho_c}(1-Z)}{m_c Z} - b = \frac{\forall_{c0} + A_{bore}V_p - \frac{m_c}{\rho_c}(1-Z) - bm_c Z}{m_c Z}$$

so that

$$p_{ave} = RT\left(\frac{1}{\frac{1}{\rho_{gas}} - b}\right) = \frac{RT\, m_c\, Z}{\forall_{c0} + A_{bore} V_p - \frac{m_c}{\rho_c}\left(1 - Z\right) - b m_c Z} \tag{3.34}$$

Free volume for the burnt gases is the difference between the total volume of empty space $\forall_{gas}$ and the volume of gas molecules.

$$\forall_{free} = \forall_{gas} - b m_c Z = \forall_{c0} + A_{bore} V_p - \frac{m_c}{\rho_c}(1 - Z) - b m_c Z \tag{3.35}$$

By the help of free volume definition, Noble-Abel equation can take the following form:

$$p_{ave} \forall_{free} = mRT \tag{3.36}$$

If igniter is written explicitly and if it is assumed that there is more than one main propellant in the chamber, the pressure equation can take the following form:

$$P_{ave} = \frac{T}{\forall_{free}}\left(\sum_{i=1}^{n} \frac{F_i m_{c_i} Z_i}{T_{0_i}} + \frac{F_{ig} m_{c_{ig}} Z_{ig}}{T_{0_{ig}}}\right) \tag{3.37}$$

3.3 Equation of Motion

In zero dimensional ballistic model, it is assumed that solid propellant grains burn in the empty volume left between breech block and base of projectile under an average pressure, p_{ave} , which is changing with the density of burnt gases in the system. However, the pressure that is acting on the base of the projectile is different than the average pressure in reality. In addition, the maximum pressure that can be measured in the chamber volume is also higher than the maximum value of the average

pressure. The reason of the difference is that the pressure acting on breech block is stagnant while the pressure is acting on the projectile is static. In other words, while the projectile is moving, there occurs a pressure gradient in the region behind the projectile. The static pressure acting at the base of the projectile and the stagnation pressure can be calculated by Lagrange model for high caliber guns in Reference [5] as:

$$p_{base} = \frac{3P_{ave} + \frac{\sum_{i=1}^{n} m_{c_i}}{m_p}\left(p_r + p_{drag}\right)}{3 + \frac{\sum_{i=1}^{n} m_{c_i}}{m_p}} \qquad (3.38)$$

$$p_{breech} = p_{base} + \frac{1}{2}\frac{\sum_{i=1}^{n} m_{c_i}}{m_p}\left(p_{base} - p_r - p_{drag}\right)$$

The previous formulas don't hold for small and medium caliber guns. To model base pressure for small and medium caliber guns, gas dynamic relations that convert stagnation pressure to static pressure can be offered as:

$$p_{breech} = p_{base}\left(1 + \left(\frac{\gamma - 1}{2}\right)\left(\frac{V_p^{\,2}}{\gamma RT}\right)\right)^{-\frac{\gamma}{\gamma - 1}} \qquad (3.39)$$

Heiney changes isentropic gas dynamic equation stated previously by averaging it from space-mean pressure with a correction factor for the deviation from isentropic behavior and [24]. The correction factor Φ is suggested to be taken as 1.5 by experimental trials.

$$p_{base} = p_{ave}\left(1 + \left(\frac{\gamma - 1}{2\Phi}\right)\left(\frac{V_p^{\,2}}{\gamma RT}\right)\right)^{-\frac{\gamma}{\gamma - 1}} \qquad (3.40)$$

When all the forces including frictional forces acting on the projectile the equation of motion becomes:

$$a_p = \frac{A_{bore}\left(p_{base} - p_r - p_{drag}\right)}{m_p} \tag{3.41}$$

In the above equation, a_p represents the acceleration of projectile. The velocity of the projectile, V_p, and the distance taken by projectile, S_p until time t can be given as:

$$V_p = \int_0^t a_p dt \tag{3.42}$$

$$S_p = \int_0^t V_p dt \tag{3.43}$$

3.4 Burn rate equation

The recession rate of propellant grains is modeled by using Vieille's burn rate equation. Vieille's law, which is also called Saint Robert's Law, is widely used in the area of solid rocket motors. According to this law, the burn rate of energetic materials is highly dependent on the pressure of the combustion chamber [19].

$$\dot{r} = B\, {p_{ave}}^n \tag{3.44}$$

In this equation, $\dot{r}$ is the linear regression rate of propellant, B is the burning rate coefficient and n is burning rate index. Therefore burn rate is a function of pressure and parameter B. It is known that parameter B is also a function of temperature. This dependence of burn rate on temperature is also known as temperature sensitivity. Erosive burning which is a function of mean flow turbulence level is not considered in this study. It should be kept in mind that mass generation of combustion gases is dependent not only on the burn rate of propellant but also on the surface area of propellant exposed to burn.

Gun propellants can have composite structure in order to shift pressure-travel curve to a desired value. Therefore, burning rate coefficient, *B*, is not constant for gun propellants. Burn rate coefficient starts from a definite value B_i and increases until a definite regression distance is reached and it becomes constant at a value of B_f [8].

All of the propellant grains are assumed to burn at the same amount under an average pressure. Therefore, all of the propellant burned until time *t* can be found by the help of linear burning distance reached at that time by the help of form factors.

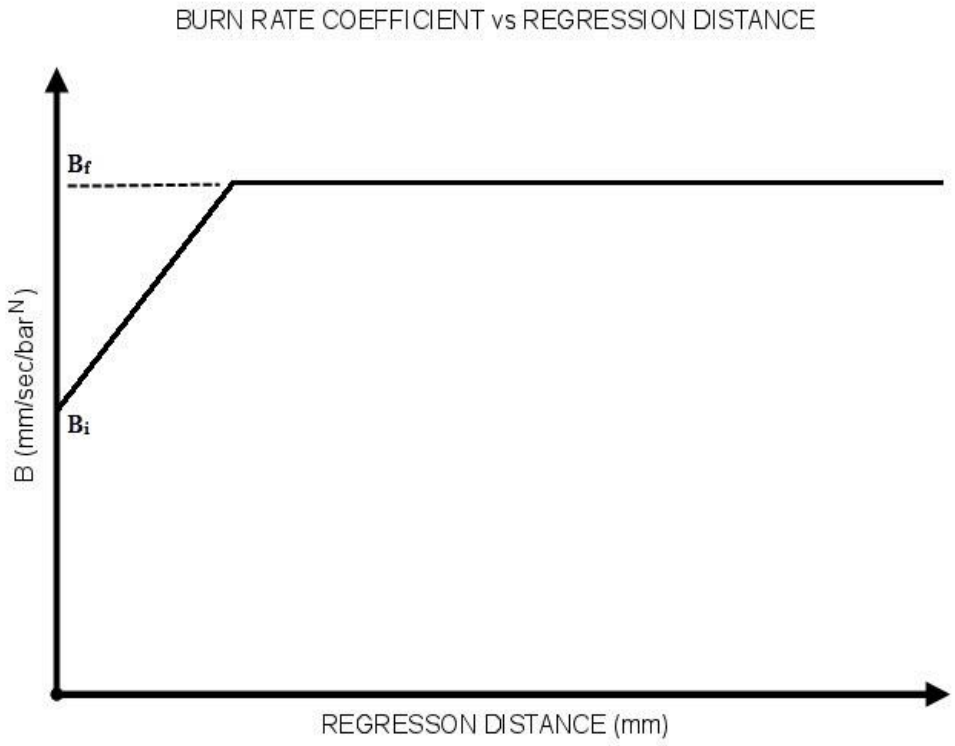

Figure 3.1 : Burn rate coefficient change of propellant

3.5 Solution Algorithm

The following steps should be applied respectively in order to solve the problem:

1) A small amount of propellant thickness r in the order of 10^{-4} mm is assumed to burn initially in order to get rid of singularity.
2) The fraction of propellant burnt (Z) is calculated.
3) Temperature, space-averaged pressure and base pressure are found.
4) Acceleration, velocity and distance of projectile are calculated
5) Regression rate of propellant is calculated and regression distance for new time step is calculated.
6) New fraction of burned propellant is calculated.
7) Steps 3 through 6 are repeated.

CHAPTER 4

ONE DIMENSIONEL MODEL

In this chapter, interior ballistics of gun is modeled as one dimensional, inviscid and real gas flow with energy and mass addition due to gradual burning of propellant. The main difference between the lumped parameter code and one dimensional model is that the pressure field with rarefaction waves is calculated directly instead of using gradient model assumptions. Since the flow in interior ballistics has high Reynolds number it is expected that Euler equations will give proper results and one-dimensional case will ease the problem in a great extent. Roe approximate Riemann solver is used for solving Euler equations and Runge-Kutta method is used for time discretization.

The instantaneous movement of the projectile in a gun barrel is similar to the rupture of diaphragm in shock tube. The rapid movement of the projectile creates a singularity that can be seen as a natural Riemann problem. Since the exact solution of the Riemann problem is available, it is commonly used in computational fluid dynamics. In addition, the solution of Riemann problem considers the condition of emerging waves. Approximate Riemann solvers are used mostly because the exact solution of the Riemann problem is required excessive computational effort.

The References [25], [26] and [27] are commonly used to construct this model.

4.1 Conservation Equations in Differential Form

Differential form of conservation of mass, momentum and energy can be written as in the following equations for one dimensional, non-viscous flow with no heat flux and body force terms.

a) Continuity equation

$$\frac{\partial \rho}{\partial t} + \frac{\partial (\rho u)}{\partial x} = 0 \tag{4.1}$$

b) Momentum equation

$$\frac{\partial u}{\partial t} + u\frac{\partial u}{\partial x} = \frac{-1}{\rho}\frac{\partial p}{\partial x} \tag{4.2}$$

c) Energy Equation

$$\frac{\partial}{\partial t}(i + \frac{u^2}{2}) + u\frac{\partial}{\partial x}(i + \frac{u^2}{2}) = -\frac{1}{\rho}\frac{\partial (up)}{\partial x} \tag{4.3}$$

In these equations i represents the internal energy per unit mass, t is the time, p is the pressure, ρ is the density and u is the velocity in x direction.

4.2 Conservation Equations in Conservative Form

a) Continuity equation

$$\frac{\partial \rho}{\partial t} + \frac{\partial (\rho u)}{\partial x} = 0 \tag{4.4}$$

b) Momentum equation

If continuity equation (4.1) is multiplied with u and the momentum equation (4.2) is multiplied with ρ and then added equation, Equation (4.5) can be obtained.

$$\frac{\partial(\rho u)}{\partial t}+\frac{\partial(\rho u^2+p)}{\partial x}=0 \tag{4.5}$$

c) Energy Equation

If the continuity equation is multiplied by $(i+u^2/2)$ and energy equation (4.3) is multiplied with ρ and then added, Equation (4.6) can be obtained.

$$\frac{\partial}{\partial t}\left[\rho(i+\frac{u^2}{2})\right]+\frac{\partial}{\partial x}\left[\rho u(i+\frac{u^2}{2}+\frac{p}{\rho})\right]=0 \tag{4.6}$$

If the total energy per unit mass, e_0, and the total energy per unit volume, E,can be written as in the following:

$$E=\rho e_0=\rho(i+\frac{u^2}{2}) \tag{4.7}$$

The enthalpy per unit mass h can be written as in the following equation:

$$h=i+\frac{p}{\rho} \tag{4.8}$$

Stagnation enthalpy per unit mass h_o can be written as in the following equation:

$$h_0=h+\frac{u^2}{2}=\frac{E+p}{\rho}=e_0+\frac{p}{\rho}=i+\frac{V^2}{2}+\frac{p}{\rho} \tag{4.9}$$

Then, Equation (4.6) can be written as in the following form:

$$\frac{\partial(\rho e_0)}{\partial t}+\frac{\partial(\rho u h_0)}{\partial x}=0 \tag{4.10}$$

If Equations (4.4), (4.5) and, (4.10) can be rearranged in the vector form as follows

$$\frac{\partial U}{\partial t}+\frac{\partial F}{\partial x}=0 \tag{4.11}$$

where U represents the solution vector of conserved variables and F is vector of conserved fluxes and given by

$$U=\begin{bmatrix}u_1\\u_2\\u_3\end{bmatrix}=\begin{bmatrix}\rho\\\rho u\\\rho e_0\end{bmatrix} \qquad F=\begin{bmatrix}f_1\\f_2\\f_3\end{bmatrix}=\begin{bmatrix}\rho u\\\rho u^2+p\\\rho u h_0\end{bmatrix} \tag{4.12}$$

By combining Equations (4.7) and (4.8) and noting that $p=\rho RT$, $h=c_pT$, $R=c_p-c_v$, $k=c_p/c_v$ and $c_p=kR/(k-1)$ for a perfect gas, the following relation can be written:

$$p=(k-1)\left[E-\frac{1}{2}\rho u^2\right]=(k-1)(\rho i) \tag{4.13}$$

4.3 Riemann Problem

The Riemann problem is a special form of the initial value problem having uniform initial conditions on an infinite spatial domain except for a single jump discontinuity. Riemann problem for one-dimensional Euler equations can be given by the following equation:

$$\frac{\partial U}{\partial t}+\frac{\partial F}{\partial x}=0 \tag{4.14}$$

with initial conditions are:

$$U(x,0)=U_0(x)=\begin{cases}U_{_L} \;\; if & x<x_0\\ U_R \;\; if & x>x_0\end{cases} \tag{4.15}$$

where U_L and U_R are left right states, respectively, at the interface.

The solution of this initial value problem can be found by using the explicit conservative formula as:

$$U_i^{\,n+1}=U_i^{\,n}-\frac{\Delta t}{\Delta x}\left(F_{i+1/2}-F_{i-1/2}\right) \tag{4.16}$$

Gudonov uses $U_{i+1/2}(0)$ which is the exact similarity solution of $U_{i+1/2}(x/t)$ and evaluates the intercell flux as $F_{i+1/2}=F(U_{i+1/2}(0))$. In Roe's method, direct approximations to the flux function is obtained and used. Equation (4.14) can be written as:

$$\frac{\partial U}{\partial t}+\frac{\partial F}{\partial x}=\frac{\partial U}{\partial t}+\frac{\partial F}{\partial U}\frac{\partial U}{\partial x}=\frac{\partial U}{\partial t}+A\frac{\partial U}{\partial x}=0 \tag{4.17}$$

where $A=\partial F/\partial U$ is called the Jacobian matrix. The Jacobian matrix is obtained by writing the flux vector in terms of the conserved variables and then partially differentiating the flux vector as:

$$F=\begin{bmatrix} u_2 \\ \frac{u_2^{\,2}}{u_1}+(\gamma-1)(u_4-\frac{u_2^{\,2}}{2u_1}) \\ \frac{u_2u_4}{u_1}+(\gamma-1)(\frac{u_2u_4}{u_1}-\frac{u_2^{\,3}}{2u_1^{\,2}}) \end{bmatrix} \tag{4.18}$$

$$\frac{\partial F}{\partial U} = A = \begin{bmatrix} \frac{\partial f_1}{\partial u_1} & \frac{\partial f_1}{\partial u_2} & \frac{\partial f_1}{\partial u_3} \\ \frac{\partial f_2}{\partial u_1} & \frac{\partial f_2}{\partial u_2} & \frac{\partial f_2}{\partial u_2} \\ \frac{\partial f_3}{\partial u_1} & \frac{\partial f_3}{\partial u_2} & \frac{\partial f_3}{\partial u_3} \end{bmatrix} \tag{4.19}$$

Here, *"a"* indicates the speed of sound. A self-similar solution, which depends only on one independent variable (i.e. *x/t*) of Riemann problem, exists if the eigenvalues of Jacobian matrix are all real and eigenvectors are complete.

As it can be seen from Equation (4.19), the elements of the Jacobian matrix is nonlinear. Linearity is desired to simplify the problem, since in non-linear systems the characteristic lines won't be parallel introducing shockwaves and expansion fans into solution. Therefore, a linear system of equations that approximates the nonlinear Euler equations is needed. If Jacobian matrix *(A)* is assumed to consist constants, Equation (4.17) becomes a system of linear equations. In addition, if Jacobian matrix is considered as diagonalizable with constant values, it can be written as:

$$A = Q\Lambda Q^{-1} \tag{4.20}$$

In this equation Q is a matrix whose columns shows the right eigen vectors of Jacobian matrix with constant elements and Q^{-1} is a matrix whose rows shows the left eigen vectors of Jacobian matrix. The matrix Λ is a diagonal matrix whose diagonal elements indicate the eigen values, λ_i,of the Jacobian matrix. If Equation (4.17) is multiplied with Q^{-1}, the following equation can be obtained:

$$\frac{\partial V}{\partial t} + \Lambda \frac{\partial V}{\partial x} = 0 \tag{4.21}$$

where V is the characteristic variable vector obtained from conserved variables as:

$$V = Q^{-1}U \tag{4.22}$$

with the initial conditions;

$$V(x,0) = \begin{cases} V_L = Q^{-1}U_L & x < 0 \\ V_R = Q^{-1}U_R & x > 0 \end{cases} \tag{4.23}$$

Now the system of linear equations is converted to scalar, independent equations in terms of characteristic variables and can be evaluated separately. Since the matrix of Q^{-1} consists of constant elements, the following relation can be written:

$$Q^{-1}\Delta U = \Delta V \tag{4.24}$$

where $\Delta V = V_R - V_L$ and $\Delta U = U_R - U_L$. To develop a numerical method, the following form should be constructed.

$$V(x,t) = V(\frac{x}{t}) = \begin{cases} V_L = V_R - \Delta V_3 - \Delta V_2 - \Delta V_1 & x/t < \lambda_3 < \lambda_2 < \lambda_1 \\ V_L + \Delta V_3 = V_R - \Delta V_2 - \Delta V_1 & \lambda_3 < x/t < \lambda_2 < \lambda_1 \\ V_L + \Delta V_3 + \Delta V_2 = V_R - \Delta V_1 & \lambda_3 < \lambda_2 < x/t < \lambda_1 \\ V_L + \Delta V_3 + \Delta V_2 + \Delta V_1 = V_R & \lambda_3 < \lambda_2 < \lambda_1 < x/t \end{cases} \tag{4.25}$$

where;

$$\Delta V_3 = \begin{bmatrix} 0 \\ 0 \\ \Delta v_3 \end{bmatrix}, \Delta V_2 = \begin{bmatrix} 0 \\ \Delta v_2 \\ 0 \end{bmatrix} \textit{ and } \Delta V_1 = \begin{bmatrix} \Delta v_1 \\ 0 \\ 0 \end{bmatrix} \tag{4.26}$$

$$\Delta V_1 + \Delta V_2 + \Delta V_3 = \Delta V = V_R - V_L \tag{4.27}$$

The solution set can be converted to conserved variables by using $U=QV$. It should be noted that every column of matrix Q represents the eigen vectors of the Jacobian matrix. In the equation stated below r_i is the i^{th} eigenvector of Jacobian matrix.

$$Q\Delta V_i = r_i \Delta v_i \tag{4.28}$$

$$U(x,t) = U(\frac{x}{t}) = \begin{cases} U_L = U_R - r_3\Delta v_3 - r_2\Delta v_2 - r_1\Delta v_1 & x/t < \lambda_3 < \lambda_2 < \lambda_1 \\ U_L + r_3\Delta v_3 = U_R - r_2\Delta v_2 - r_1\Delta v_1 & \lambda_3 < x/t < \lambda_2 < \lambda_1 \\ U_L + r_3\Delta v_3 + r_2\Delta v_2 = U_R - r_1\Delta v_1 & \lambda_3 < \lambda_2 < x/t < \lambda_1 \\ U_L + r_3\Delta v_3 + r_2\Delta v_2 + r_1\Delta v_1 = U_R & \lambda_3 < \lambda_2 < \lambda_1 < x/t \end{cases} \tag{4.29}$$

The flux at the boundaries of each cell is also required for the numerical solution of Euler equations. The fluxes of each face will be investigated separately so that *x/t* can be taken as zero for the respective face of the cell. By the help of Equation (4.30), the flux vector can be written as:

$$Ar_i = \lambda_i r_i \tag{4.30}$$

$$F(0) = \begin{cases} AU_L = AU_R - r_3\lambda_3\Delta v_3 - r_2\lambda_2\Delta v_2 - r_1\lambda_1\Delta v_1 & x/t < \lambda_3 < \lambda_2 < \lambda_1 \\ AU_L + r_3\lambda_3\Delta v_3 = AU_R - r_2\lambda_2\Delta v_2 - r_1\lambda_1\Delta v_1 & \lambda_3 < x/t < \lambda_2 < \lambda_1 \\ AU_L + r_3\lambda_3\Delta v_3 + r_2\lambda_2\Delta v_2 = AU_R - r_1\lambda_1\Delta v_1 & \lambda_3 < \lambda_2 < x/t < \lambda_1 \\ AU_L + r_3\lambda_3\Delta v_3 + r_2\lambda_2\Delta v_2 + r_1\lambda_1\Delta v_1 = AU_R & \lambda_3 < \lambda_2 < \lambda_1 < x/t \end{cases} \tag{4.31}$$

A simpler form can be given as follows:

$$\begin{aligned} F(0) &= AU_L + \sum_{i=1}^{n} r_i\lambda_i^{-}\Delta v_i \quad with\ \lambda_i^{-} = \min(0,\lambda_i) \\ F(0) &= AU_R - \sum_{i=1}^{n} r_i\lambda_i^{+}\Delta v_i \quad with\ \lambda_i^{+} = \max(0,\lambda_i) \end{aligned} \tag{4.32}$$

The sign of eigen values vanishes by taking an average as:

$$F(0) = \underbrace{\frac{1}{2}A(U_L + U_R)}_{\frac{1}{2}[F(U_L)+F(U_R)]} - \frac{1}{2}\sum_{i=1}^{N} r_i\left|\lambda_i\right|\Delta v_i \tag{4.33}$$

4.4 Roe Riemann Solver

In Roe's approximate Riemann solver, the Jacobian matrix is approximated by using an average state from left and right states. The average state are derived by selecting an appropriate parameter vector as in the following:

$$L = \begin{pmatrix} l_1 \\ l_2 \\ l_3 \end{pmatrix} = \sqrt{\rho} \begin{pmatrix} 1 \\ u \\ h_0 \end{pmatrix} \tag{4.34}$$

The flux vector and the conserved variable vector are quadratic in terms of L. In addition, the average of parameter vector of left and right states, $\overline{L}$, should be defined to express differences between left and right states of flux and conserved variable vector.

$$\overline{L} = \begin{bmatrix} \overline{l_1} \\ \overline{l_2} \\ \overline{l_3} \end{bmatrix} = \frac{1}{2}\left(L_L + L_R\right) = \begin{bmatrix} \sqrt{\rho_L} + \sqrt{\rho_R} \\ \dfrac{\sqrt{\rho_L}u_L + \sqrt{\rho_R}u_L}{2} \\ \dfrac{\sqrt{\rho_L}h_{0L} + \sqrt{\rho_R}h_{0R}}{2} \end{bmatrix} \tag{4.35}$$

The parameter vector allows to express the difference of left and right states of conserved variables, ΔU as

$$\Delta U = B\Delta L \tag{4.36}$$

where,

$$B = \begin{bmatrix} 2\overline{l_1} & 0 & 0 \\ \overline{l_2} & \overline{l_1} & 0 \\ \dfrac{\overline{l_3}}{\gamma} & \dfrac{\gamma-1}{\gamma}\overline{l_2} & \dfrac{\overline{l_1}}{\gamma} \end{bmatrix} \tag{4.37}$$

The difference of flux vector can also be expressed similarly as;

$$\Delta F = C\Delta L \tag{4.38}$$

where,

$$C = \begin{bmatrix} \bar{l}_2 & \bar{l}_1 & 0 \\ \frac{\gamma-1}{\gamma}\bar{l}_3 & \frac{\gamma+1}{\gamma}\bar{l}_2 & \frac{\gamma-1}{\gamma}\bar{l}_1 \\ 0 & \bar{l}_3 & \bar{l}_2 \end{bmatrix} \tag{4.39}$$

The flux vector and the conserved variable vector can be related as:

$$\Delta F = CB^{-1}\Delta U \tag{4.40}$$

where CB^{-1} can be seen as Jacobian matrix,A, in terms of average state. The eigen values and right eigen vectors of Jacobian matrix are as:

$$\bar{\lambda}_1 = \bar{u} + \bar{a} \qquad \bar{\lambda}_2 = \bar{u} \qquad \bar{\lambda}_3 = \bar{u} - \bar{a} \tag{4.41}$$

$$r_1 = \begin{bmatrix} 1 \\ \bar{u} + \bar{a} \\ \bar{h}_0 + \bar{u}\bar{a} \end{bmatrix} \qquad r_2 = \begin{bmatrix} 1 \\ \bar{u} \\ \frac{\bar{u}^2}{2} \end{bmatrix} \qquad r_3 = \begin{bmatrix} 1 \\ \bar{u} - \bar{a} \\ \bar{h}_0 - \bar{u}\bar{a} \end{bmatrix} \tag{4.42}$$

where Roe averaged variables for ideal gases are:

$$\begin{aligned} \bar{\rho} &= \sqrt{\rho_L \rho_R} \\ \bar{u} &= \frac{\bar{l}_2}{\bar{l}_1} = \frac{\sqrt{\rho_L}u_L + \sqrt{\rho_R}u_R}{\sqrt{\rho_L} + \sqrt{\rho_R}} \\ \bar{h}_0 &= \frac{\bar{l}_3}{\bar{l}_1} = \frac{\sqrt{\rho_L}h_{0L} + \sqrt{\rho_R}h_{0R}}{\sqrt{\rho_L} + \sqrt{\rho_R}} \\ \bar{a} &= \sqrt{(\gamma-1)(\bar{h}_0 - \frac{\bar{u}^2}{2})} \end{aligned} \tag{4.43}$$

By using the inverse of new representation of eigen vector matrix and Equation (4.24), the characteristic variables which is also called wave strengths take the form:

$$\overline{V} = \begin{bmatrix} \dfrac{(\Delta p - \overline{\rho}\,\overline{a}\,\Delta u)}{2\overline{a}^{2}} \\ \dfrac{(\overline{a}^{2}\Delta\overline{\rho} - \Delta p)}{\overline{a}^{2}} \\ \dfrac{(\Delta p + \overline{\rho}\,\overline{a}\,\Delta u)}{2\overline{a}^{2}} \end{bmatrix} \tag{4.44}$$

To solve the problem, fistly left and right states should be computed. Secondly, the Roe averages must be calculated. Thirdly, the wave speeds should be calculated. Fourthly, the wave strength and right eigen vectors should be calculated. Lastly, the flux relation in (4.33) should be evaluated.

4.5 Application of Equation of State

The equation of state for real gases is different from ideal gases. Therefore, the conservative variable vector and flux vector will be different due to covolume parameter. The specific internal energy and speed of sound terms are in the following form for real gases [27]:

$$\begin{aligned} p &= \frac{(\gamma - 1)\rho i}{(1 - b\rho)} \\ a &= \sqrt{\frac{\gamma p}{(1 - \mathrm{b}\,\rho)\rho}} \end{aligned} \tag{4.45}$$

Roe averaged states should be written in terms of these parameters which includes covolume. Covolume takes a value of $0.9\text{x}10^{-3} \leq b \leq 1.1\text{x}10^{-3}$ m^3/kg. Flux vector in Equation (4.18) takes the following form for real gases as

$$F=\begin{bmatrix} f_1 \\ f_2 \\ f_3 \end{bmatrix}=\begin{bmatrix} u_2 \\ \dfrac{u_2{}^2}{u_1}+\dfrac{(\gamma-1)\left(u_3-\dfrac{1}{2}\dfrac{u_2{}^2}{u_1}\right)}{(1-b*\mathrm{u}_1)} \\ \dfrac{u_2}{u_1}\left(u_3+\dfrac{(\gamma-1)\left(u_3-\dfrac{1}{2}\dfrac{u_2{}^2}{u_1}\right)}{(1-b*\mathrm{u}_1)}\right) \end{bmatrix} \tag{4.46}$$

If Jacobian matrix is calculated as in Equation (4.19), the eigen values for real gases is obtained as:

$$\begin{aligned} \lambda_1 &= \frac{u_2}{u_1} \\ \lambda_2 &= \frac{2u_1^2u_2-4bu_1^3u_2+2b^2u_1^4u_2-\sqrt{2}\sqrt{(-1+\gamma)\gamma u_1^4(-1+bu_1)^2(-u_2^2+2u_1u_3)}}{2u_1^3(-1+bu_1)^2} \\ \lambda_3 &= \frac{2u_1^2u_2-4bu_1^3u_2+2b^2u_1^4u_2+\sqrt{2}\sqrt{(-1+\gamma)\gamma u_1^4(-1+bu_1)^2(-u_2^2+2u_1u_3)}}{2u_1^3(-1+bu_1)^2} \end{aligned} \tag{4.47}$$

and the right eigenvectors for real gases can be seen in Equations (4.50),(4.51) and (4.52). After the right eigen vector matrix is evaluated, the left eigen vector matrix can be found by taking the inverse of it. Then, the characteristic variable vectors can be calculated using the Equation (4.24). In addition, the flux can be calculated by using Equations (4.20) and (4.31) with the known eigen values and eigen matrix.

4.6 Grid Generation and Boundary Conditions

Computational domain between the breech block and base of projectile is discretized with finite number of cells to initiate the algorithm before the ignition takes place. When the projectile starts moving, the number of cells will be increased according to the position of projectile. If the distance taken by projectile while moving forward along the barrel exceeds the length of initial cells, the number of cells will be increased by one. The flux of last cell with varying volume is calculated Arbitrary Lagrangian Eulerian Method. In Figure 4.1, the spatial discretization of problem is illustrated.

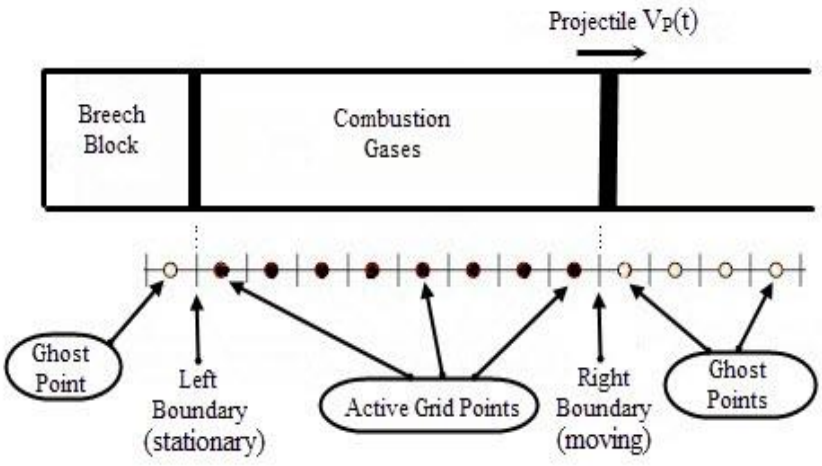

Figure 4.1 : Discretization of computational domain

Ghost cells are used to find the properties at the boundaries which can be seen in Figure 4.1. The breech block at the rear part of gun acts as a stationary wall. Therefore, the average of velocities of ghost cell and first cell should be equal to zero at the face of the breech block. The boundary conditions at breech block can be taken as:

$$\rho_0^{\,n} = \rho_1^{\,n} \;,\quad u_0^{\,n} = -u_1^{\,n} \;,\quad p_0^{\,n} = p_1^{\,n} \tag{4.48}$$

The projectile can be thought as a moving wall. The average of velocities of last cell and ghost cell at the face of projectile base should be equal to velocity of projectile. The boundary conditions at the base of projectile can be taken as:

$$\rho_{M+1}^{\ n} = \rho_M^{\ n} \ , \ \ u_{M+1}^{\ n} = -u_M^{\ n} + 2V_p \ \ , \ \ p_{M+1}^{\ n} = p_M^{\ n} \tag{4.49}$$

4.7 Source Terms and Time Discretization

In the developed code, an initial number of cells is assigned to chamber volume and propellant grains are always kept burning in these cells. Therefore, the volume of cells is increasing due to decrease in the volume of solid propellant grains. In addition, there is mass and energy addition emerged from burning propellant grains into these cells. The increase in volume, mass addition and energy addition occurs as source term in the formulations. Conservation laws which have been written in strong form (i.e. differential formulation) are used to solve Riemann problem, so far. However, weak form of conservation laws (i.e. integral form) is used in order to add mass and energy and volume addition into the system at each time step.

Fourth order Runge-Kutta time stepping technique is used for time discretization.

$$r_1 = \begin{bmatrix} \dfrac{2u_1^2(-1+bu_1)}{-u_2^2+2bu_1^2u_3} \\ \dfrac{2u_1(-1+bu_1)u_2}{-u_2^2+2bu_1^2u_3} \\ 1 \end{bmatrix} \tag{4.50}$$

$$r_2 = \begin{bmatrix} \dfrac{2u_1^2(-1+bu_1)\left(-2(-1+\gamma)u_1^2u_2+2b(-1+\gamma)u_1^3u_2-\sqrt{2}\sqrt{(-1+\gamma)\gamma u_1^4(-1+bu_1)^2(-u_2^2+2u_1u_3)}\right)}{-2b(-1+\gamma)u_1^3u_2^3-4b(-1+\gamma)u_1^4u_2u_3+4b^2(-1+\gamma)u_1^5u_2u_3-3\sqrt{2}(-1+\gamma)u_2^2\sqrt{(-1+\gamma)\gamma u_1^4(-1+bu_1)^2(-u_2^2+2u_1u_3)}+2\sqrt{2}\gamma u_1u_3\sqrt{(-1+\gamma)\gamma u_1^4(-1+bu_1)^2(-u_2^2+2u_1u_3)}+2u_1^2\left((-1+\gamma)u_2^3-\sqrt{2}bu_3\sqrt{(-1+\gamma)\gamma u_1^4(-1+bu_1)^2(-u_2^2+2u_1u_3)}\right)} \\ \dfrac{\left(2(-1+\gamma)u_1^2u_2-2b(-1+\gamma)u_1^3u_2+\sqrt{2}\sqrt{(-1+\gamma)\gamma u_1^4(-1+bu_1)^2(-u_2^2+2u_1u_3)}\right)\left(-2u_1^2u_2+4bu_1^3u_2-2b^2u_1^4u_2+\sqrt{2}\sqrt{(-1+\gamma)\gamma u_1^4(-1+bu_1)^2(-u_2^2+2u_1u_3)}\right)}{u_1(-1+bu_1)(-2b(-1+\gamma)u_1^3u_2^3-4b(-1+\gamma)u_1^4u_2u_3+4b^2(-1+\gamma)u_1^5u_2u_3-3\sqrt{2}(-1+\gamma)u_2^2\sqrt{(-1+\gamma)\gamma u_1^4(-1+bu_1)^2(-u_2^2+2u_1u_3)}+2\sqrt{2}\gamma u_1u_3\sqrt{(-1+\gamma)\gamma u_1^4(-1+bu_1)^2(-u_2^2+2u_1u_3)}+2u_1^2\left((-1+\gamma)u_2^3-\sqrt{2}bu_3\sqrt{(-1+\gamma)\gamma u_1^4(-1+bu_1)^2(-u_2^2+2u_1u_3)}\right))} \\ 1 \end{bmatrix} \tag{4.51}$$

$$r_3 = \left[\begin{array}{c} \dfrac{\left(-2\left(-1+\gamma\right)u_1^2u_2 + 2b\left(-1+\gamma\right)u_1^3u_2 + \sqrt{2}\sqrt{\left(-1+\gamma\right)\gamma u_1^4\left(-1+bu_1\right)^2\left(-u_2^2+2u_1u_3\right)}\right)2u_1^2u_2 - 4bu_1^3u_2 + 2b^2u_1^4u_2 + \sqrt{2}\sqrt{\left(-1+\gamma\right)\gamma u_1^4\left(-1+bu_1\right)^2\left(-u_2^2+2u_1u_3\right)})}{u_1\left(-1+bu_1\right)(-2b\left(-1+\gamma\right)u_1^3u_2^3 - 4b\left(-1+\gamma\right)u_1^4u_2u_3 + 4b^2\left(-1+\gamma\right)u_1^5u_2u_3 + 3\sqrt{2}\left(-1+\gamma\right)u_2^2\sqrt{\left(-1+\gamma\right)\gamma u_1^4\left(-1+bu_1\right)^2\left(-u_2^2+2u_1u_3\right)} - 2\sqrt{2}\gamma u_1u_3\sqrt{\left(-1+\gamma\right)\gamma u_1^4\left(-1+bu_1\right)^2\left(-u_2^2+2u_1u_3\right)} + 2u_1^2\left(\left(-1+\gamma\right)u_2^3 + \sqrt{2}bu_3\sqrt{\left(-1+\gamma\right)\gamma u_1^4\left(-1+bu_1\right)^2\left(-u_2^2+2u_1u_3\right)}\right))} \\ \\ \dfrac{\left(-2\left(-1+\gamma\right)u_1^2u_2 + 2b\left(-1+\gamma\right)u_1^3u_2 + \sqrt{2}\sqrt{\left(-1+\gamma\right)\gamma u_1^4\left(-1+bu_1\right)^2\left(-u_2^2+2u_1u_3\right)}\right)2u_1^2u_2 - 4bu_1^3u_2 + 2b^2u_1^4u_2 + \sqrt{2}\sqrt{\left(-1+\gamma\right)\gamma u_1^4\left(-1+bu_1\right)^2\left(-u_2^2+2u_1u_3\right)})}{u_1\left(-1+bu_1\right)\left(-2b\left(-1+\gamma\right)u_1^3u_2^3 - 4b\left(-1+\gamma\right)u_1^4u_2u_3 + 4b^2\left(-1+\gamma\right)u_1^5u_2u_3 + 3\sqrt{2}\left(-1+\gamma\right)u_2^2\sqrt{\left(-1+\gamma\right)\gamma u_1^4\left(-1+bu_1\right)^2\left(-u_2^2+2u_1u_3\right)} - 2\sqrt{2}\gamma u_1u_3\sqrt{\left(-1+\gamma\right)\gamma u_1^4\left(-1+bu_1\right)^2\left(-u_2^2+2u_1u_3\right)} + 2u_1^2\left(\left(-1+\gamma\right)u_2^3 + \sqrt{2}bu_3\sqrt{\left(-1+\gamma\right)\gamma u_1^4\left(-1+bu_1\right)^2\left(-u_2^2+2u_1u_3\right)}\right)\right)} \\ \\ 1 \end{array} \right] \tag{4.52}$$

CHAPTER 5

RESULTS AND DISCUSSION

In this chapter, the verification of 0D and 1D model are presented and the differences between the ideal gas flow assumption and real gas flow are examined. Firstly, the results of 0D and 1D model under the case of the immobile projectile are given to ensure the validity of the written code; in addition, the results for both Noble-Abel equation of state and ideal gas equation of state are given separately to examine the differences between the cases of ideal gas flow and real gas flow. Secondly, the outputs of 0D and 1D model are examined under the case of moving projectile for both ideal gas and real gas flow in order to see the tendency of velocity and the effect of selected pressure gradient.

The inputs data required for the developed code and used in test case can be seen in Table 5.1 through 5.5. The propellant grains are selected as single perforated and inhibited in length (i.e. propellant grains are only allowed to decrease only in width). In addition, it is assumed that there is no igniter propellant, no heat losses and no frictional losses in the system unless otherwise is stated. Effective weight formula in Equation (3.15) is also taken into account in the solver.

Table 5.1 : Igniter Propellant Properties

Impetus (MJ/kg)	0.4982
Specific Heat Ratio	1.2
Flame Temperature (K)	3400
Mass (g)	0.0324

Table 5.2 : Properties of Projectile and Barrel Tube

Projectile Mass (g)	9.4876
Barrel Tube length (cm)	60.96
Chamber Volume (cm^3)	3.27761
Bore Diameter (mm)	7.62
Bore Area (mm^2)	46.972
Pidduck-Kent Constant	3.05

Table 5.3 : Properties of Main Propellant

Impetus (MJ/kg)	0.98
Bi ($cm/s/bar^N$)	0.05507
Slope ($1/s/bar^N$)	8.08691
Bf ($cm/s/bar^N$)	0.10213
Burn Rate Index	0.69
Covolume (cm^3/g)	1.0
Specific Heat Ratio	1.24
Flame Temperature (K)	2825
Mass (g)	2.6762
Type of Propellant	Single Perforated
Outer Diameter of Grain(mm)	0.9398
Inner Diameter of Grain (mm)	0.4064
Length of Grain (mm)	2.1336
Web Thickness of Grain (mm)	0.2667

Table 5.4 : Resistance Profile along Barrel Tube

Travel (mm)	*Pressure (MPa)*
0.0	7.57
1.45	52.30
5.81	52.30
7.26	35.10
10.9	24.78
29.06	14.45
72.65	9.29
217.95	7.57
435.9	5.85
14530.0	5.85

Table 5.5 : Other Parameters for Algorithm

Euler Time Stepping (ms)	1.0E-04
CFL Number	0.1
Initial Number of Cells	100
Time Delay(ms)	0.0
Ambient Temperature (K)	300
Estimation for Muzzle Velocity (m/s)	869.0
Number of Propellants	1

5.1 Comparison of 0D and 1D Model for Ideal Gas Flow

5.1.1 Ideal Gas Flow Results for the Case of Immobile Projectile

In this section, the variation of pressure and temperature of burnt gases with time for 0D and 1D models with ideal gas and stationary projectile assumptions are indicated in Figure 5.1 and Figure 5.2, respectively.

Ideal gas equation of state ignores the volume of gas particles. Therefore, when all the propellant burns, it is expected that the available volume for burnt gases should changes from chamber volume excluding the volume of the initial propellants $(\forall_{c0} - m_{c0}/\rho_c)$ to chamber volume, $\forall_{c0}$, which is 3.2776 cm^3 for the test case and can be seen in Figure 5.1.

Since the projectile is assumed as stationary, base pressure acting on the projectile is expected to be equal to space-average pressure of lumped parameter code when considering Heiney pressure gradient. However, a little difference between average pressure and base pressure is expected for 1D model due to pressure gradient between cells. In addition, the value of average pressure is expected to reach approximately 800 Mpa as observed from Figure 5.1 which can also be calculated by using the following equation:

$$p_{\max} = \frac{F_c\, m_{c0}}{\forall_{c0}} \tag{5.1}$$

Furthermore, if a very small value of covolume like (10^{-8} m^3/kg) is introduced into the 1D code, the result must be consistent with 0D model to verify the program.

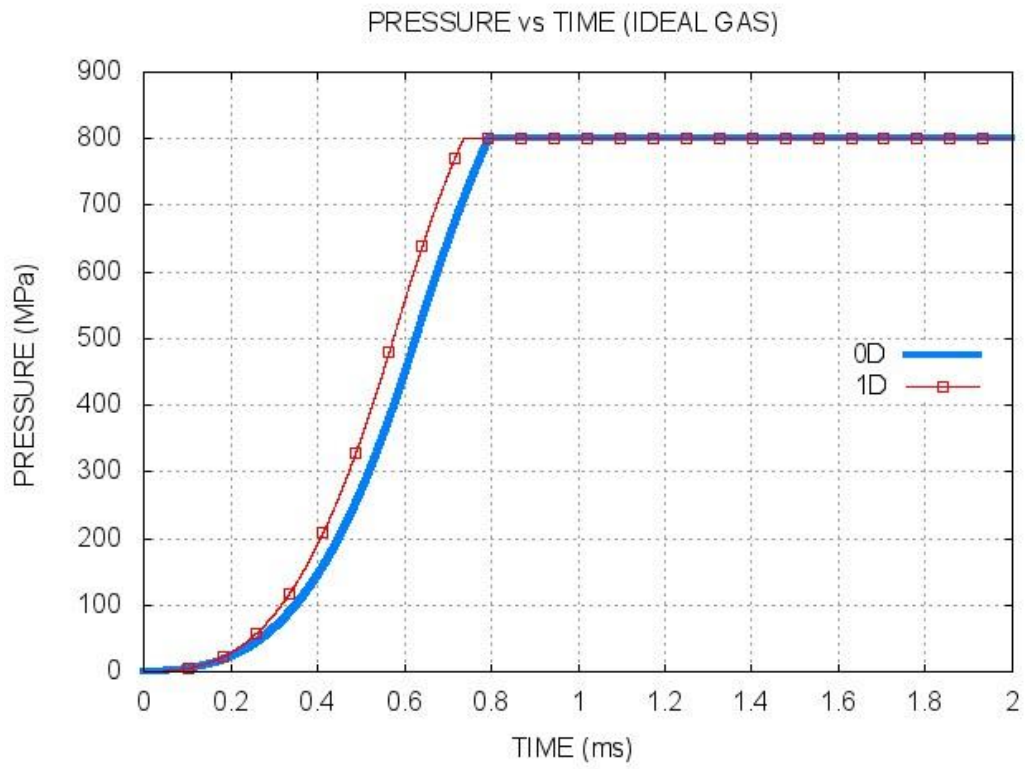

Figure 5.1: Variation of the space averaged pressure and base pressure acting on projectile with time for an immobile projectile case (ideal gas)

It is assumed that the system is adiabatic and no work done by the system since the projectile is stationary. Therefore, the temperature is expected to be constant since there exists no losses and the temperature in system should be equal to flame temperature of the propellant due to burning for 0D model as observed in Figure 5.2. In zero dimensional model, the volume behind the projectile at t=0 is considered as vacuum according to formulations. In 1D model, it is considered that there exists air with initial conditions at ambient (P=100Kpa, T=300K) at the volume behind projectile at t=0. For this reason, the temperature calculated in 1D model starts from initial temperature and increases due to enthalpy addition and finally reaches to the flame temperature of the propellant. In addition, the final tempetature in 1D model is

seen as 2823K which is a little lower than flame temperature of propellant. Some energy spent on heating the air in the chamber volume can be said as a reason of lower temperature compared to 0D model.

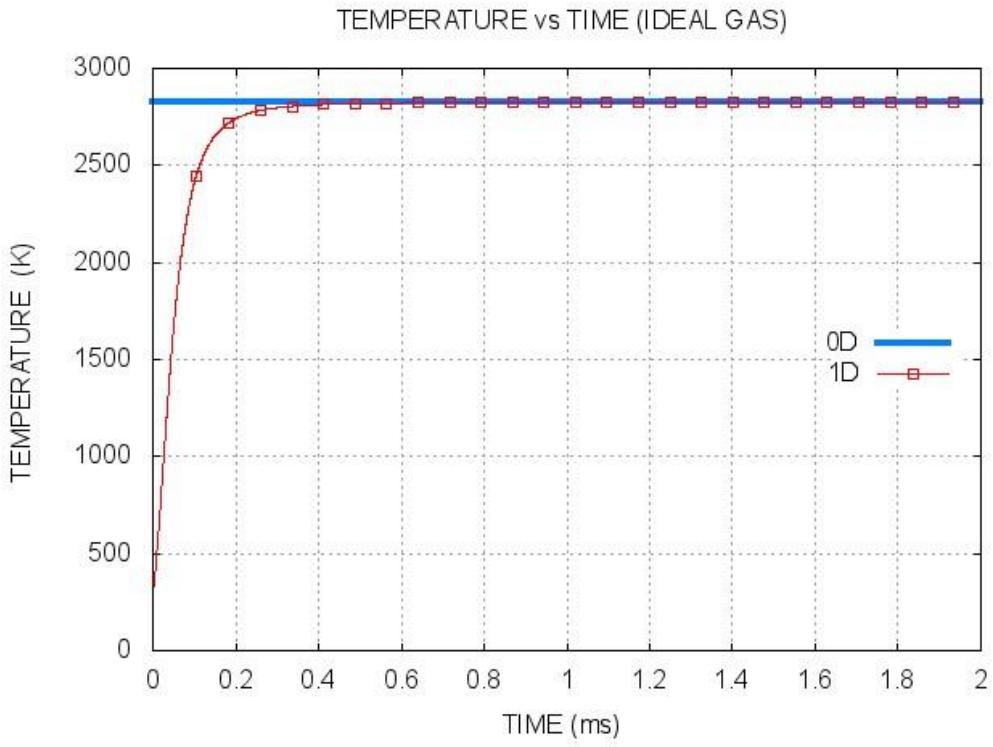

Figure 5.2: Variation of the temperature of chamber volume with time for an immobile projectile case (ideal gas)

5.1.2 Ideal Gas Flow Results for the Case of Moving Projectile

In this section, the variation of pressure and temperature results of burnt gases and velocity of the moving projectile with time for models when the gas is taken as ideal, are presented in Figures 5.3, 5.5 and 5.6, respectively. The base pressure acting on projectile can be seen in Figure 5.4. The difference between average pressure and base pressure is due to the pressure gradient. In 1D model, greater peak pressure is occurred and the propellant mass is burnt quickly (at $t \approx$ 1ms) than 0D model (at $t \approx$ 1.2 ms).

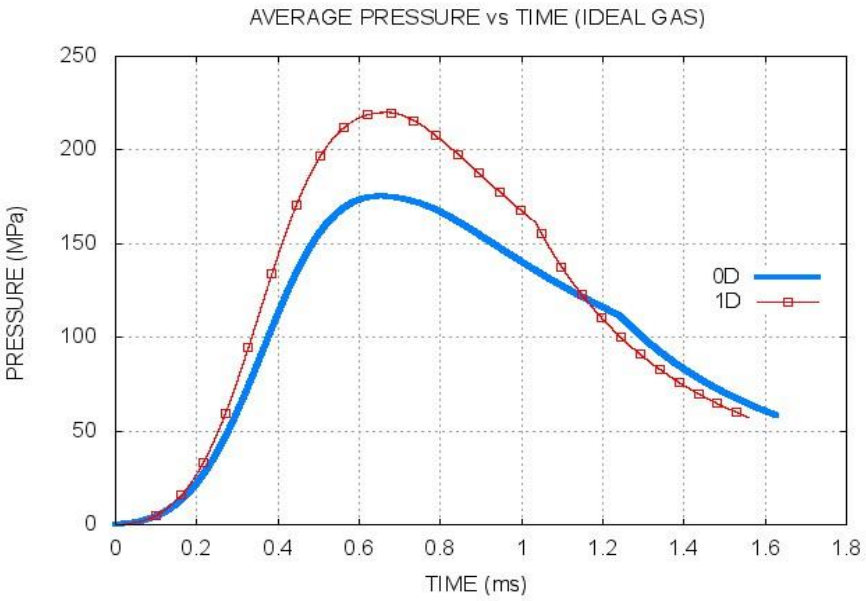

Figure 5.3 : Variation of the average pressure with time for a moving projectile case (ideal gas)

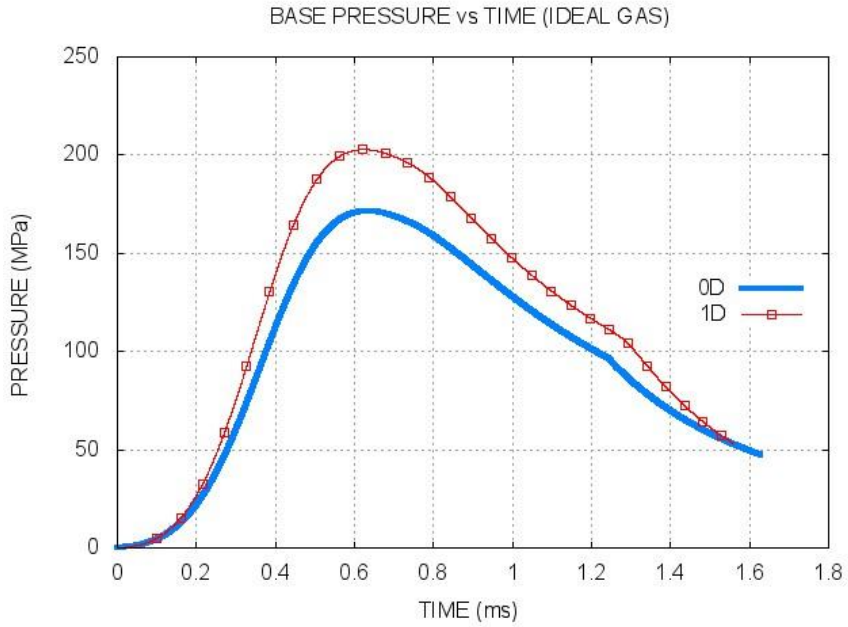

Figure 5.4 : Variation of the base pressure with time for a moving projectile (ideal gas)

After ignition, it is expected that the temperature rise to flame temperature of propellant from ambient temperature. In addition, the temperature is expected to fall after a while since there is work done by system while moving the projectile. There is nearly %30 of energy given to the movement of projectile. Since the expansion of projectile is more rapid in 1D case due to high pressure, it is also expected that the temperature fall greater with time when compared to 0D case. In addition, the temperature of combustion gases should be slightly bigger like 2835K than flame temperature of propellant in 1D model when considering peak values. In 1D model with mobile projectile, there emerges waves that can heat the volume behind the projectile when compared to 1D model with immobile projectile. In addition, it shouldn't be forgotten that 1D model can also show the effect of adiabatic compression of combustion gases in contrast to 0D model.

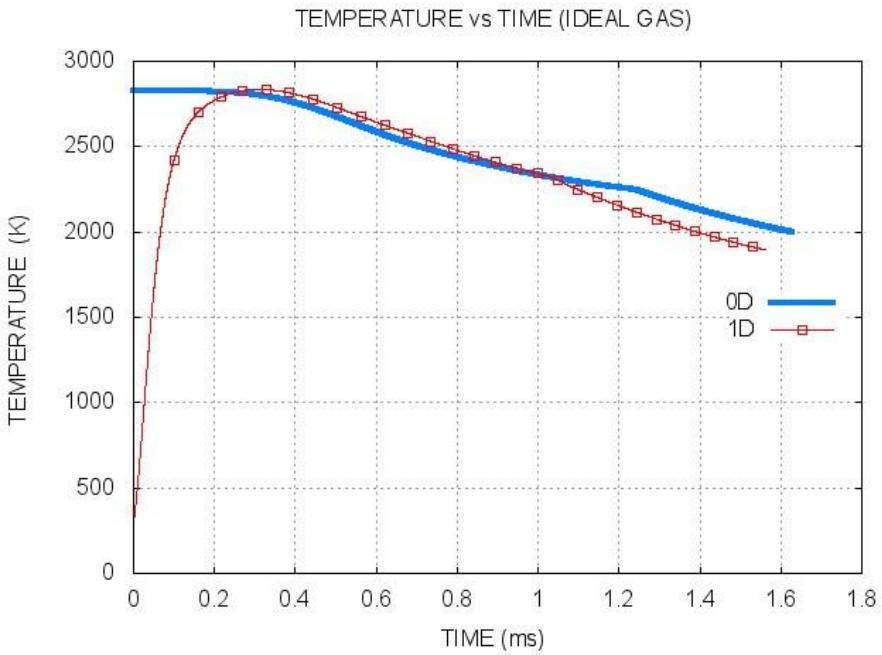

Figure 5.5 : Variation of temperature of burnt gases with time for a moving projectile (ideal gas)

The velocity at the muzzle reaches nearly 800 m/s when the gas is treated as ideal . After 0.6 ms the pressure tends to decrease and therefore the rate of increase in velocity is expected to decrease as observed from Figure 5.6.

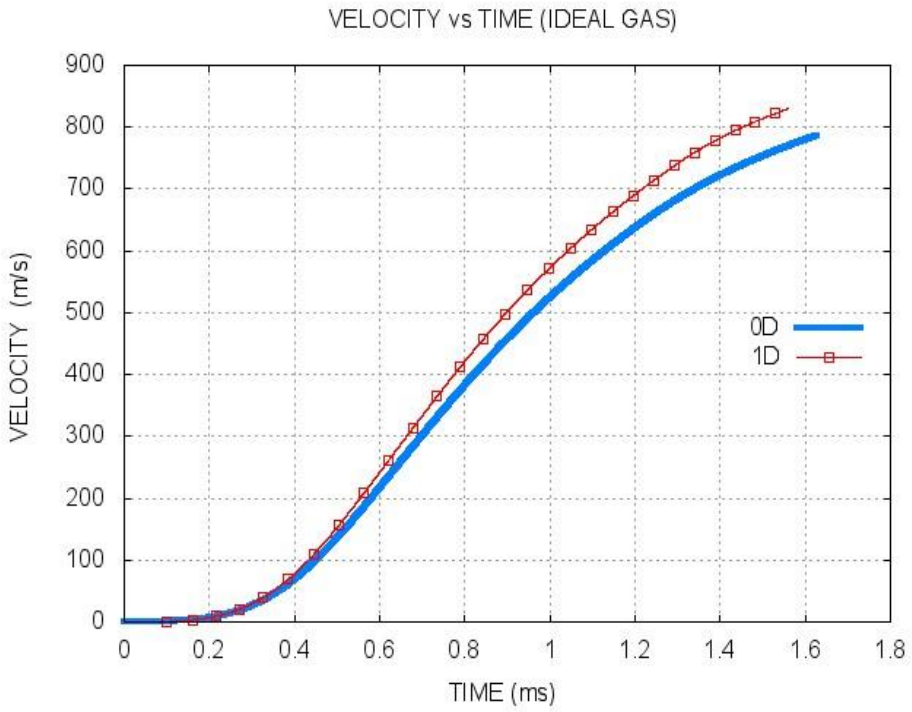

Figure 5.6 : Variation of the velocity of projectile with time (ideal gas)

5.2 Comparison of 0D and 1D Model When the Burnt Gases are treated as Real

5.2.1 Immobile Projectile When the Burnt Gases are treated as Real

In this section, variation of the pressure and temperature of the burnt gases with time for an immobile projectile when the burnt gases are treated as real, are shown in Figures 5.7 and 5.8, respectively.

The firing of a gun is so sudden and the mass of gas per unit volume increases enormously in a very short time. Therefore, the volume occupied by gas particles can't be neglected to obtain realistic results. Noble-Abel equation of state (i.e. real gas equation of state) takes into account of the volume of gas particles by introducing covolume. A covolume of 1 cm^3/g given in the literature introduces a significant affect for an immobile projectile.

In addition, since the free volume available for the gases decreases while the propellant is burning, greater pressure values are expected when the burnt gases are treated as real. By using the following equation,

$$P_{\max} = \frac{F_c\, m_{c0}}{\forall_{c0} - b * m_{c0}} \tag{5.2}$$

maximum pressure is expected to be approximately 4300 MPa as observed from Figure 5.7.

Since the projectile is assumed as stationary, the base pressure acting on the projectile is expected to be equal to the space averaged pressure of the lumped parameter code. Since the propellant is burning at flame temperature and there is no loss to environment by any means, the temperature is expected to be equal to flame temperature as observed from Figure 5.8.

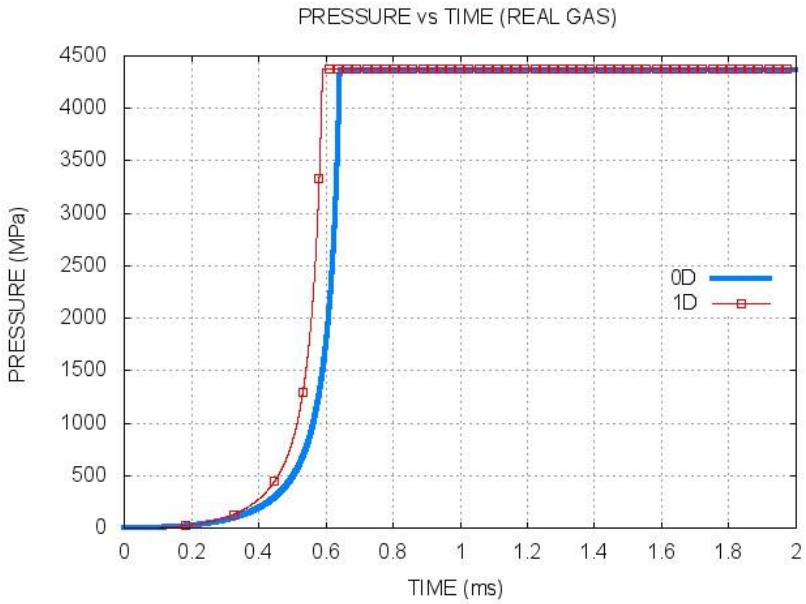

Figure 5.7 : Variation space averaged pressure and base pressure acting on the projectile with time for an immobile projectile (real gas)

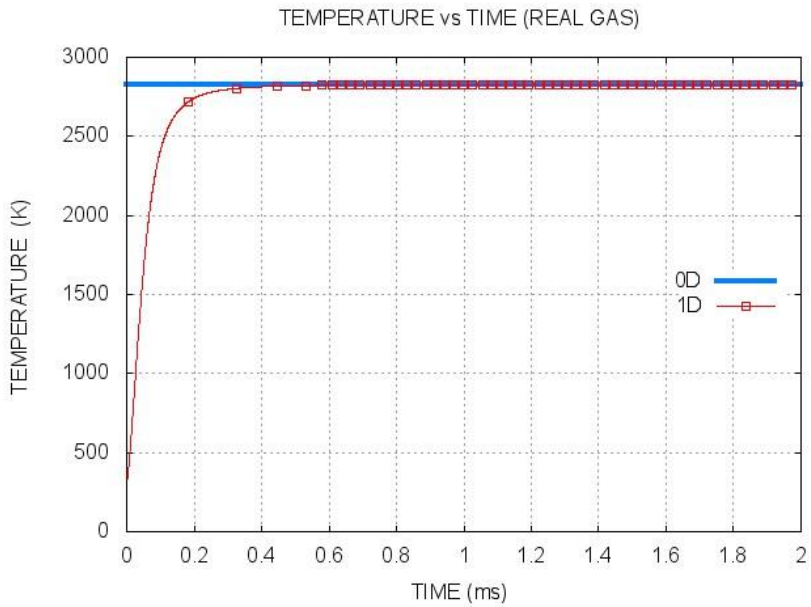

Figure 5.8 : Variation of the chamber temperature and velocity of the projectile with time for an immobile projectile (real gas)

5.2.2 Real Gas Flow Results for the Case of Moving Projectile

In this section, variation of the pressure and temperature of the burnt gases and the velocity of the moving projectile with 0D and 1D are shown in Figures 5.9, 5.11 and 5.12, respectively. The variation of the base pressure of the moving projectile is presented in Figure 5.10. Modeling the flow as real is expected to give higher pressure velocity results and lower muzzle reaching since it has a decreasing effect on volume that is available for burnt gases. By comparing the pressure for ideal gas assumption in Figure 5.3 with the pressure for real gas flow in Figure 5.9, the effect of covolume can be seen.

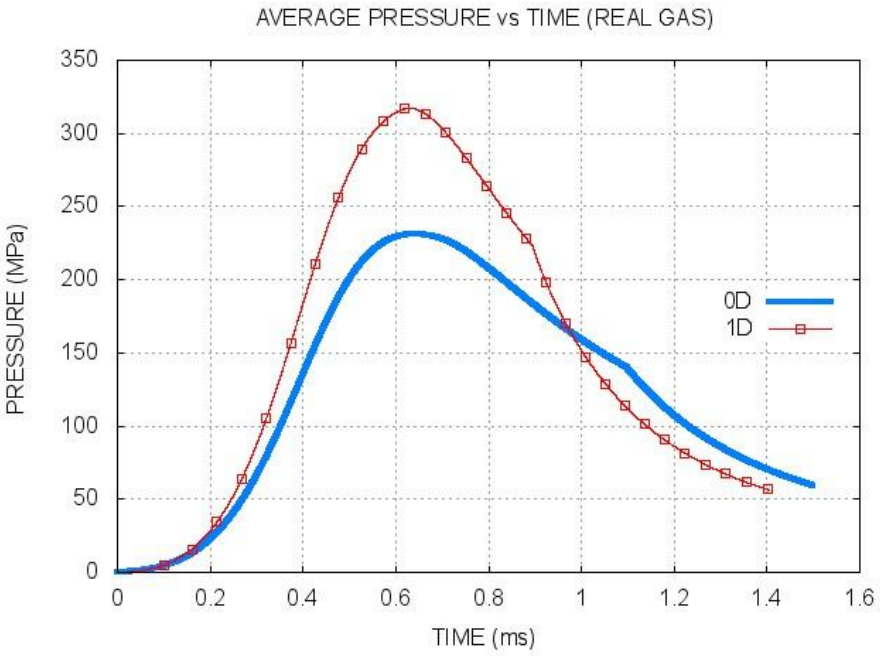

Figure 5.9: Variation of the average pressure of burnt gases with time for a moving projectile case (real gas)

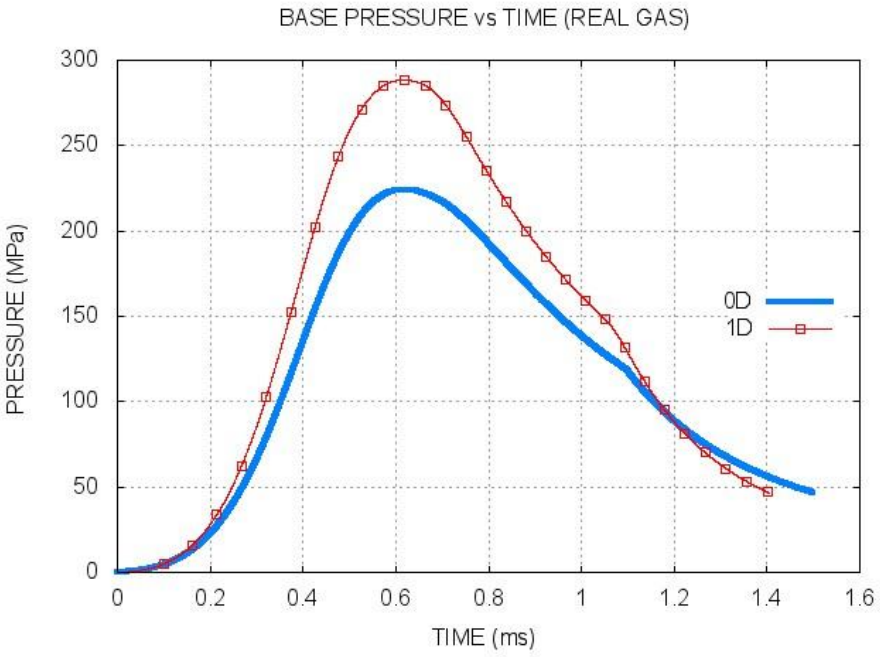

Figure 5.10 : Variation of the base pressure with time for a moving projectile (real gas)

Since work is done by the system to move the projectile, the temperature is expected to decrease.The velocities at the muzzle are not very different from each other for 0D and 1D cases despite the differences seen in pressure curves. Since 1D case reaches higher pressure values at early times, it is expected that the time required for the projectile to reach the muzzle in 1D case is less than the 0D case. After 0.6 ms, the pressure tends to decrease; therefore, the rate of increase in velocity is expected to decrease, as observed from Figure 5.12.

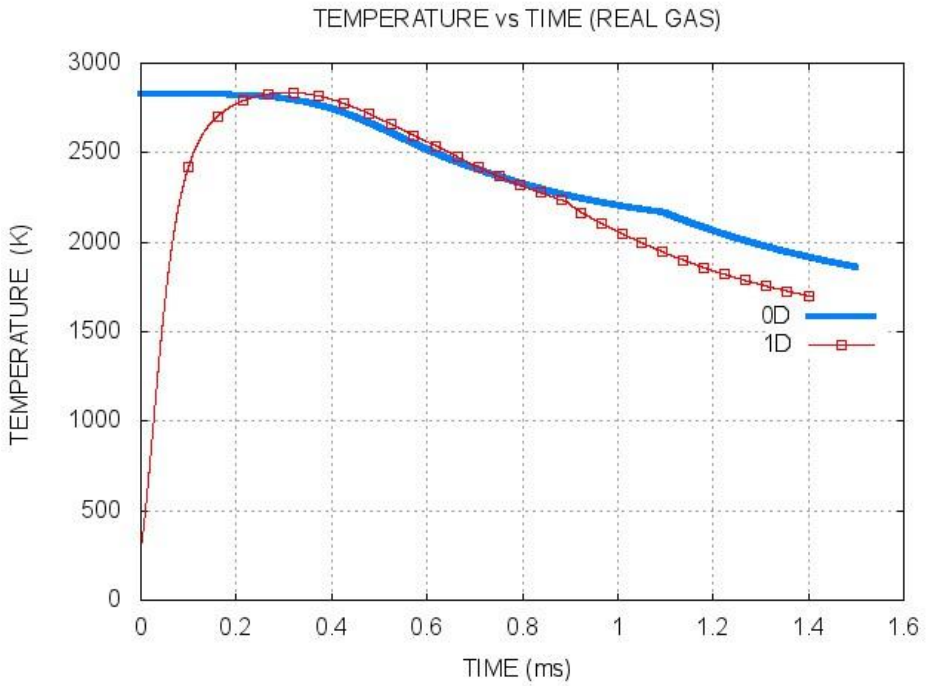

Figure 5.11 : Variation of the temperature of burnt gases with time for a moving projectile (real gas)

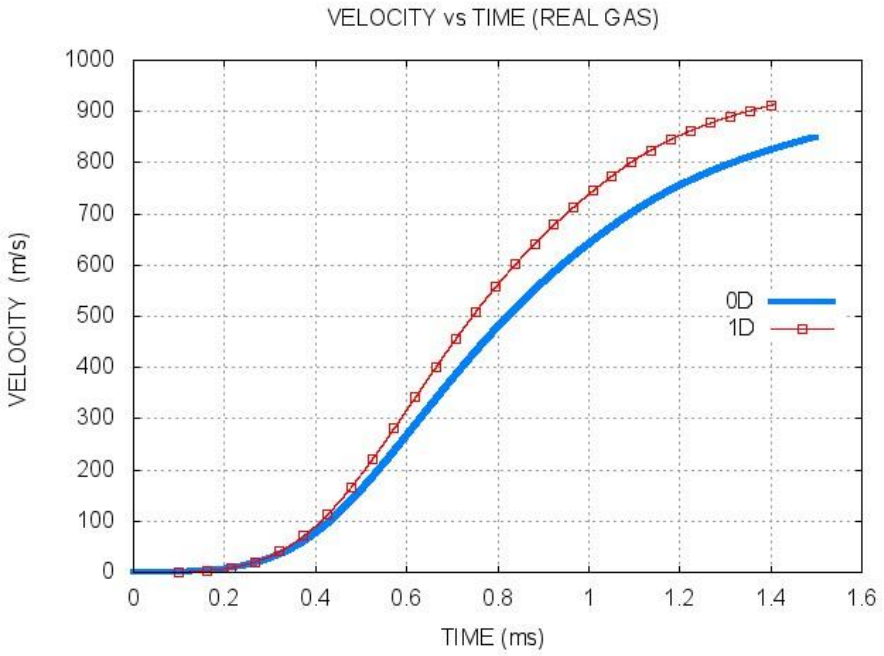

Figure 5.12 : Variation of the velocity of the projectile with time (real gas)

5.2.3 Real Gas Flow Results for the Case of Moving Projectile with Resistance Profile

In this section, variation of the pressure and temperature of the burnt gases and the velocity of the moving projectile with 0D and 1D are shown for a barrel tube having friction in Figures 5.13, 5.16 and 5.17, respectively. The variation of the base pressure of the moving projectile is presented in Figure 5.14 and the resistive pressure due to frictional forces defined in Table 5.4 is presented in Figure 5.15. The engraving force is simulated as 52 MPa*A_{bore} and acts along the length of 5 mm, which is very small when compared to barrel length. However, it increases the peak pressure from 300 MPa in Figure 5.9 to 400 MPa, which shows the importance of introducing resistive forces into the model in order to converge real cases in riffled guns. Increased pressure reflects as an increase in velocity of projectile as predicted.

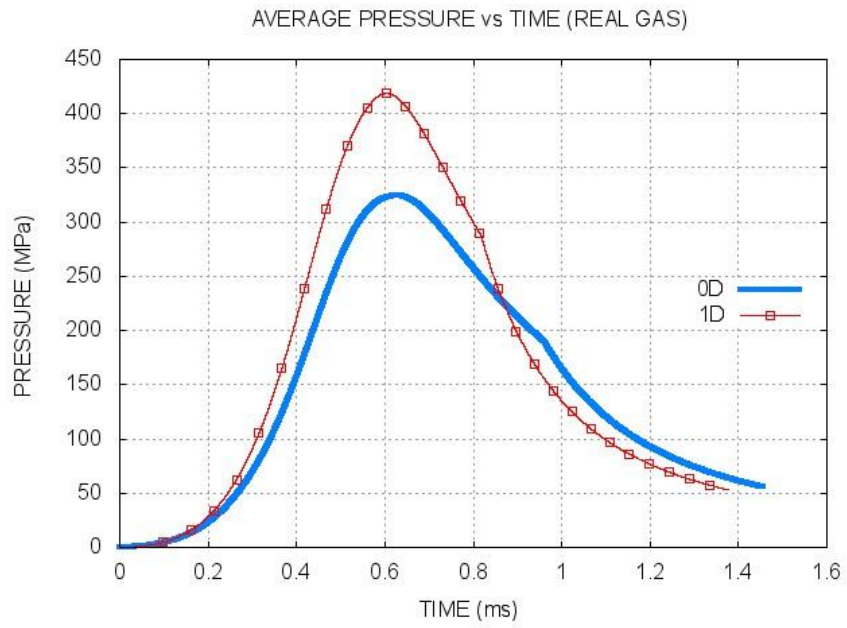

Figure 5.13: Variation of the average pressure with time for a moving projectile and frictional barrel tube (real gas)

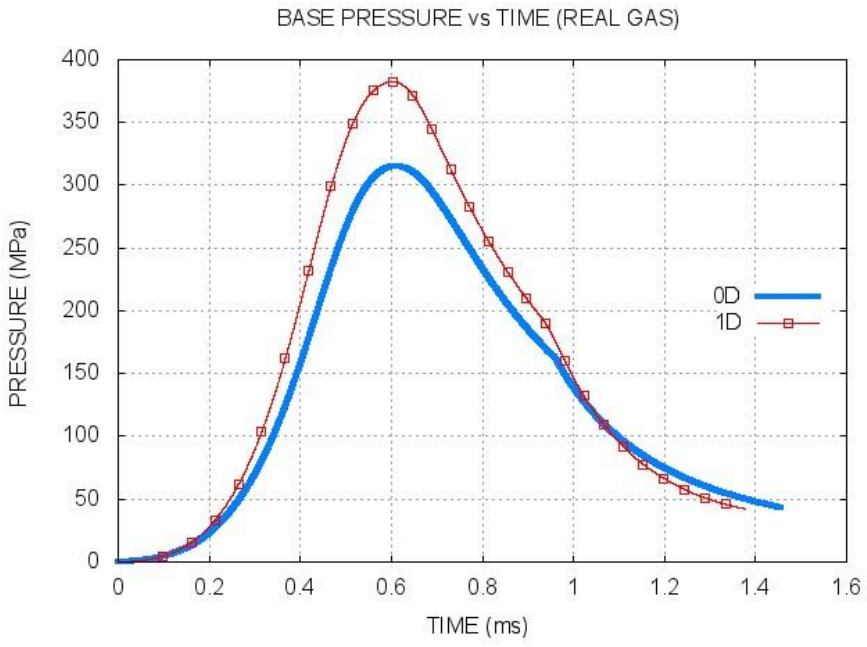

Figure 5.14: Variation of the base pressure with time for a moving projectile and frictional barrel tube (real gas)

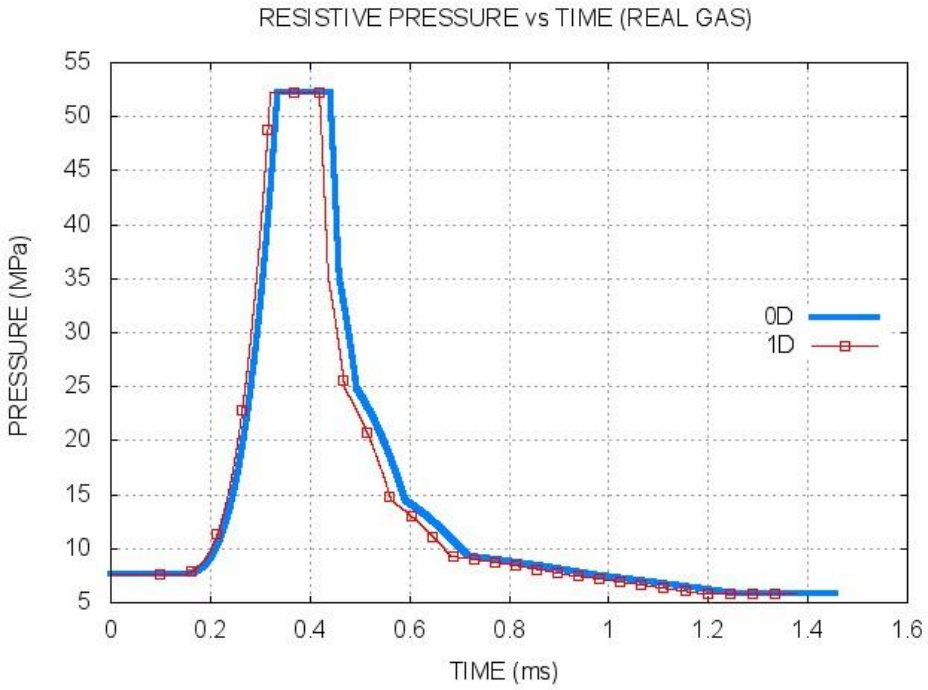

Figure 5.15: Variation of the resistive pressure with time for a moving projectile and frictional barrel tube (real gas)

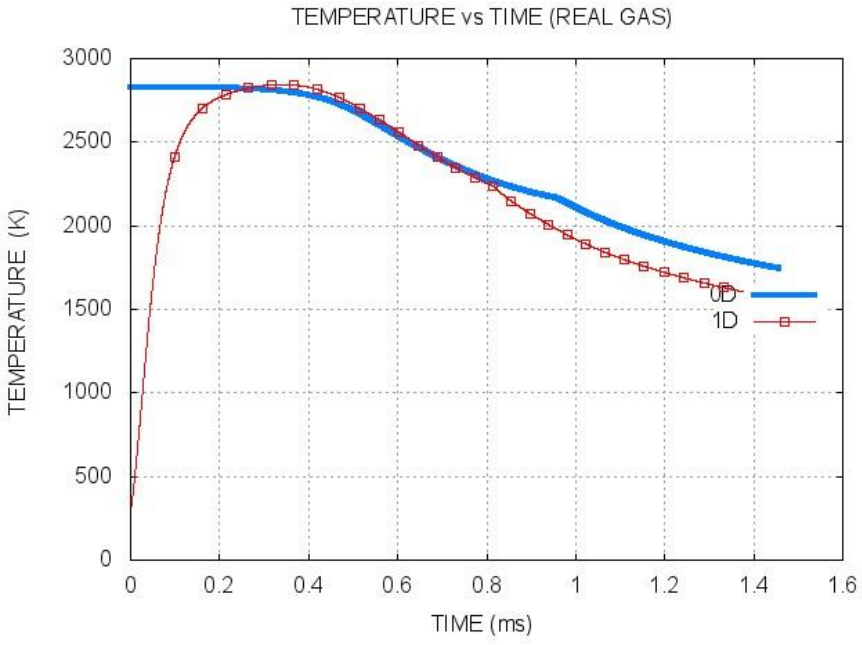

Figure 5.16: Variation of the temperature with time for a moving projectile with frictional barrel tube (real gas)

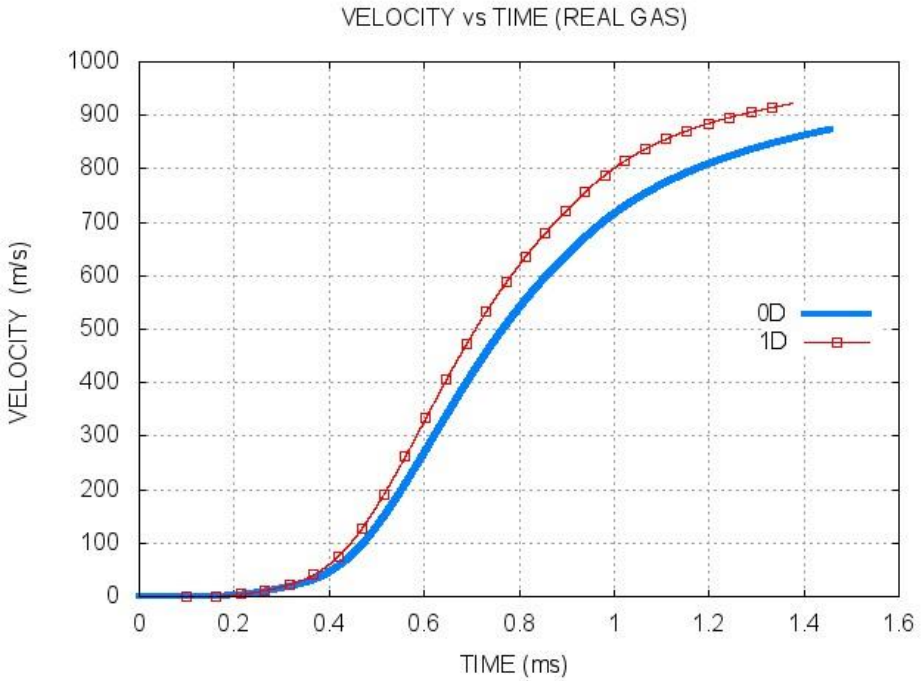

Figure 5.17: Variation of the velocity with time for a moving projectile with frictional barrel tube (real gas)

In Figure 5.18, the pressure distribution of each cell along barrel tube can be seen. For a fixed time step, it can be seen that the pressure doesn't linearly decrease from breech block to base of projectile. Increasing and then decreasing structure of pressure distribution along barrel tube shows that 1D model can simulate the effect of waves. The movement of traveling waves along barrel tube can easily be seen easily in the figure. In Figure 5.19, base pressure and projectile velocity change with projectile travel for 0D and 1D model can be seen. In this figure, it can be easily seen that the pressure of combustion gases reach peak value although the projectile travels a little distance from combustion chamber.

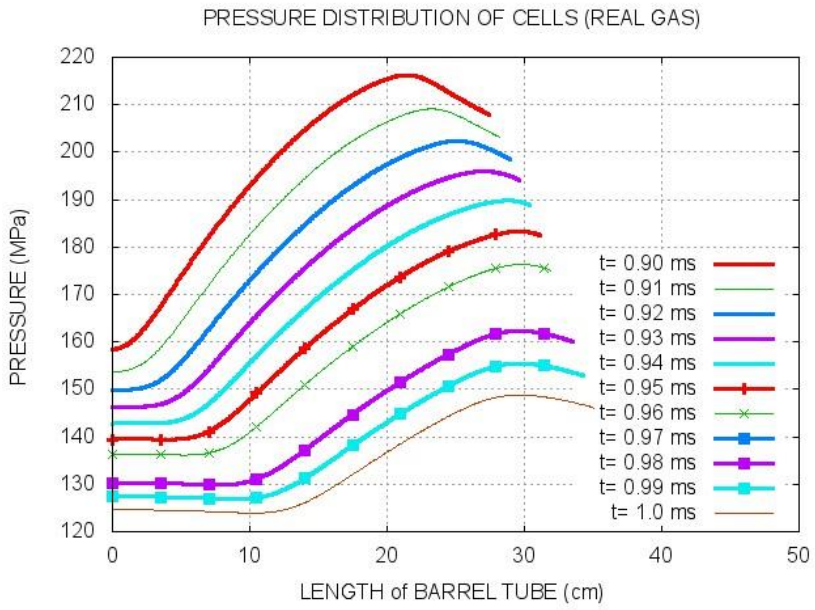

Figure 5.18 : Pressure distribution of cells along barrel tube between 0.9 and 1 ms for a moving projectile with frictional barrel tube (real gas)

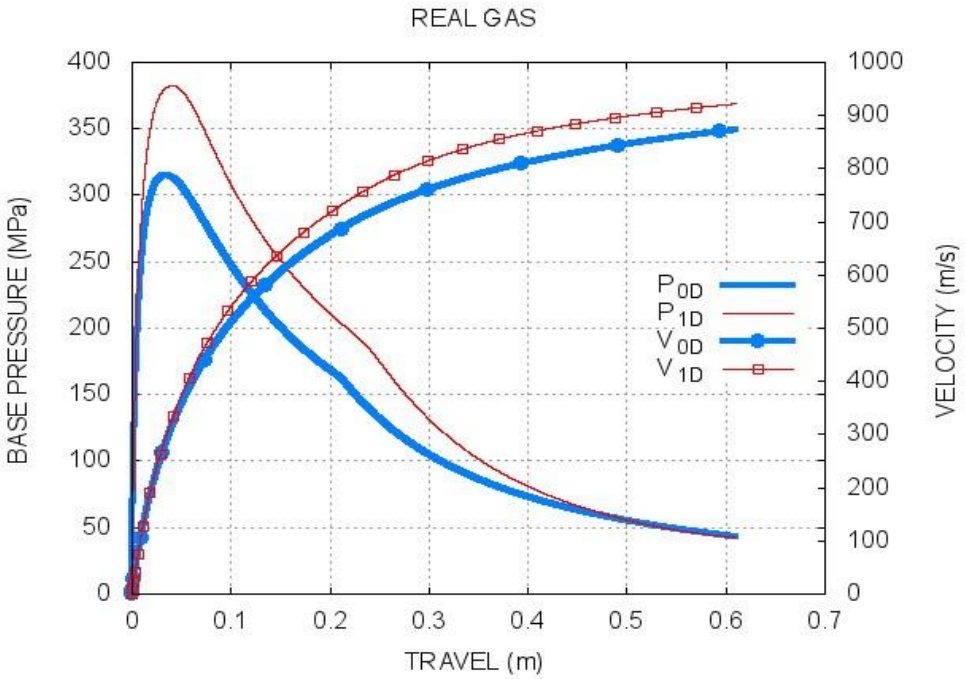

Figure 5.19: Variation of base pressure and projectile velocity with travel for a moving projectile with frictional barrel tube (real gas)

5.3 Comparison of 0D Model and PRODAS for Real Gas Flow and the Case of Moving Projectile with Resistance Profile

In this section, variation of the pressure and temperature of the burnt gases and the velocity of the moving projectile with 0D and PRODAS, which is a commercial ballistic program, are shown for a barrel tube having friction in Figures 5.18 through 5.21. The flow is modelled as real gas flow with heat losses with frictional barrel tube. The loss of heat is calculated from Equation (3.20) and the resistance profile in Table 5.4 is used to simulate friction. In these calculations, it is assumed that there exists igniter propellant which has properties stated in Table 5.1. Therefore, it should be noted that the temperature of combustion gases should start from the flame temperature of igniter propellant which is 3400K and can be seen in figures. It can be seen that the pressure and velocity results of 0D model is very consistent with PRODAS; however, there are deviations about temperature of burnt gases. It is mentioned that there are some optimizations done with temperature in Reference [8] which can be the reason behind the deviation in models.

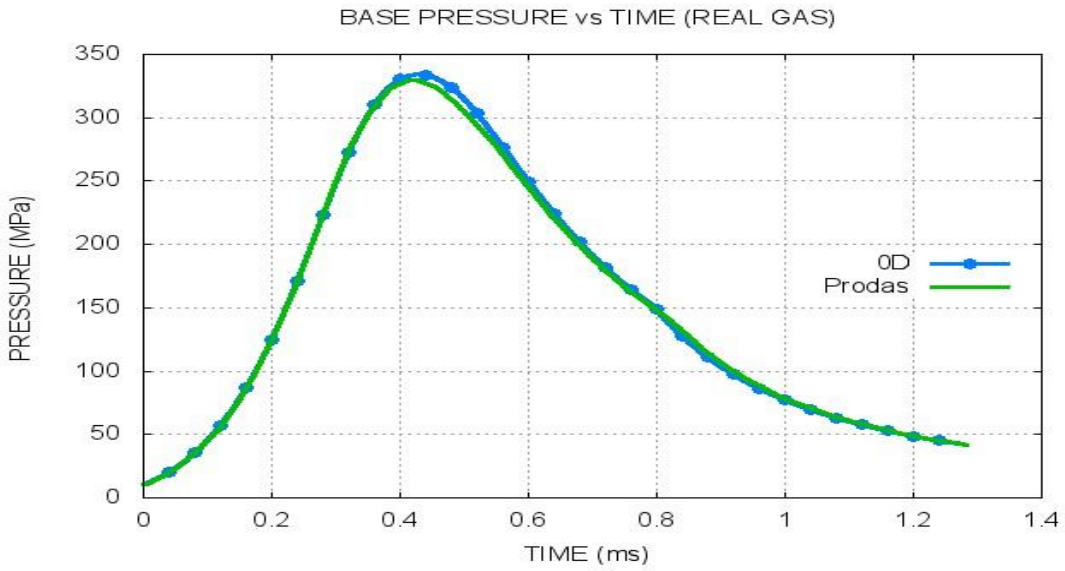

Figure 5.20: Variation of the base pressure with time for a moving projectile with frictional barrel tube (real gas)

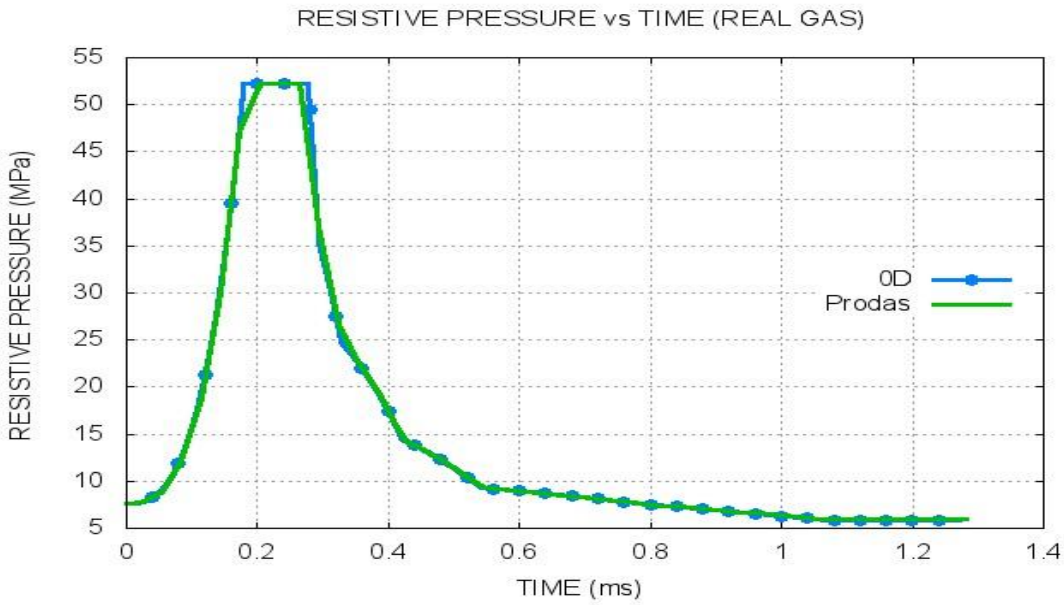

Figure 5.21: Variation of the resistive pressure with time for a moving projectile with frictional barrel tube (real gas)

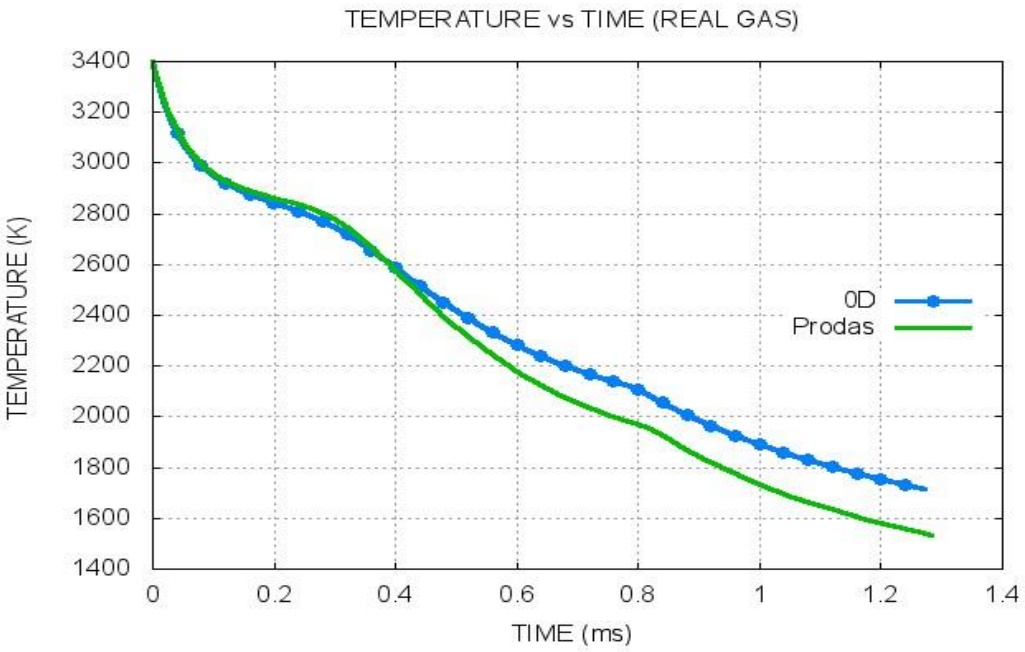

Figure 5.22: Variation of the temperature with time for a moving projectile with frictional barrel tube (real gas)

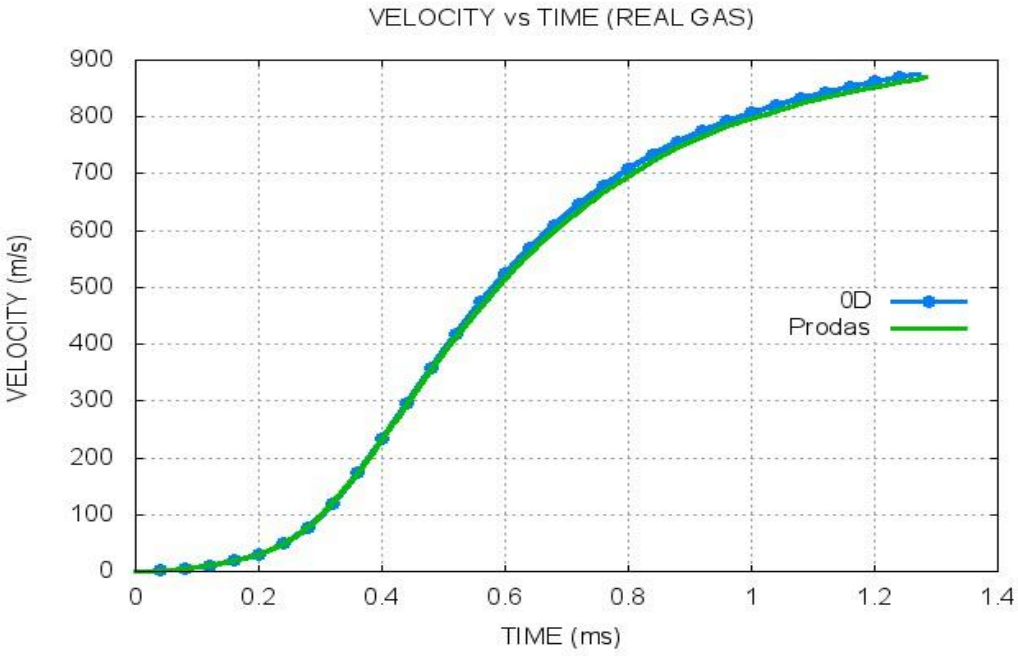

Figure 5.23: Variation of the velocity with time for a moving projectile with frictional barrel tube (real gas)

CHAPTER 6

CONCLUSION

This thesis aimed to simulate the problem of gun interior ballistics for conventional solid propellant guns. It can be considered as an initial study to improve the knowledge on interior ballistics of gun in defense industry and give deeper perspective to gun design. Also, it is gradually targeted to get rid of the commercial program used in the related industry.

In this work, the interior ballistic problem is studied as zero dimensionally and one dimensionally and two codes are produced. Gradual burning of propellant grains is considered in both codes. In zero dimensional code, lumped parameter approach, which is based on tracking the change of all parameters with the energy emerged from ignition of propellant. This method is quick as push button to get the results. In addition, it is very handful when integrating different parameters due to losses into the model. The experimental results of definite gun can also be easily integrated in this model and more correct estimations for different guns can be done. In one dimensional code, the flow is considered as inviscid and Euler equations are solved. This code is much more complex, harder to integrate parameters and have longer evaluation time like a couple of minutes. In both of the models the flow is considered as real by introducing the parameter of covolume. In one dimensional model, a great effort is done to evaluate the Jacobian matrix, eigen values and eigen vectors for real gas equation of state.

If the results of the developed models are thought, it can be clearly said that one dimensional model predicts much higher pressure values for peak values than zero dimensional model, which results in higher velocity results and earlier time to reach

model. Therefore, the results of one dimensional model should be used as a design criterion for peak values at the chamber volume in order to consider safety. In addition, zero dimensional model which gives higher base pressure values at the muzzle should be used as design criterion for barrel tube. However, lower muzzle pressure values in one dimensional model should be used in exterior ballistics in order to calculate the range of projectile. Also, it should not be forgotten that some correction factor are used in zero dimensional model in order to catch the tendency of commercial ballistic program. On the other hand, either the zero dimensional model or one dimensional model can be said to be true because only the information about muzzle velocities in commercial program are verified by defense company and there is lack of experimental results on pressure history in barrel tube. Nevertheless, the one dimensional model is believed to be more realistic.

This study can be improved by an experimental research on finding the true history for pressure results for a simple barrel tube and projectile configuration with verifying of burn rate properties of propellants on widely-used rifles in defense industry. In addition, the modeling of engraving force and friction for different bullet and riffled barrel tube configurations in industry can be studied. A two-phase flow model can be added to one-dimensional model to expand its capacity. A two-dimensional axisymmetrical model can be useful as a next step to examine the effect of larger chamber diameters than diameter of barrel tube and to examine the effect of rear end design of projectiles. An axisymmetrical model can also be used to examine the blast caused by projectile leaving muzzle and to study sound emission as a further step.

REFERENCES

[1] Corner, J, "Theory of Interior Ballistics of Guns", John Wiley & Sons Inc., New York, USA, 1950.

[2] Kapur, J. N., "Lagrange's Ballistic Problem for Unorthodox Guns and Solid Fuel Rockets, Delhi University, Delhi, 1957.

[3] Oberle, W.F., Morrison, W.F. and Wren, G.P., "The Application of Lagrange and Pidduck-Kent Gradient Models to Guns using Low Molecular Weight Gases", Army Research Laboratory(ARL), 1993.

[4] Horst, A., "A Brief Journey Through the History of Gun Propulsion", Army Research Laboratory, 2005.

[5] Baer, P.G. and Frankle, J.M., "The Simulation of Interior ballistic Performance of Guns by Digital Computers", Ballistic Research Laboratory, 1962.

[6] Stiefel, L., "Gun propulsion Technology", Progress in Astronautics and Aeronautics, Volume 109, 1979.

[7] Anderson, R.D and Fickie, K.D., "IBHVG2 User's Guide", 1987.

[8] Arrow Tech. Associates, "Projectile Design and Analysis System (PRODAS) Manual"

[9] Oberle, F. "Constant Pressure Interior Ballistic Code CONPRESS: theory and User's Manual", Army Research Laboratory, 1993.

[10] Gough, P.S., “The XNOVAKTC Code”, Ballistic Research Laboratory, 1990.

[11] Nussbaum, J., Helluy, P., Herard J.M.., Carriere A., “Numerical Simulations of Gas-Particle Flows with Combustion”, 2005.

[12] Miura, H. Matsuo, A., Nakamura, Y., “Numerical Prediction of Interior Ballistics Performance of Projectile Accelerator Using Granular or Tubular Solid Propellant”, “Propellants, Explosives,Pyrotechnics”, 2012.

[13] Lowe, C., “CFD Modeling of Solid Propellant Ignition”, Cranfield University, 1996.

[14] Acharya, R., “Modeling AND Numerical Simulation of Interior Ballistic processes in a 120mm Mortar System”, The Pennsylvania State University, 2009.

[15] Gough, P., “Initial Development of Core Module of Next Generation Interior Ballistic Model”, 1995.

[16] Allsop, D.F and Toomey, M.A., “Small Arms General Design“, 1999.

[17] Öztürk, A.R., “İç Balistik”, Makina ve Kimya Endüstrisi Kurumu Genel Müdürlüğü Özel Yayınları, Ankara, 1984.

[18] U.S Army Material Command, “ Engineering Design Handbook, Ammunition Series”, North Carolina, USA, 1964.

[19] Krier, H. and Adams, M.J., “An Introduction to Gun Interior Ballistics and a Simplified Ballistic Code”, Interior Ballistics of Guns, Volume 66, New York, USA, 1979.

[20] U.S Army Material Command, “Interior Ballistics of Guns”,Engineering Design Handbook Ballistic Series, 1965.

[21] Baer, P.G., “Practical Interior Ballistic Analysis of Guns”, Interior Ballistics of Guns, Progress in Astronautics and Aeronautics, Volume 66, New York, USA, 1979.

[22] Siewert, J., Cytron, S., “Riffling Profile Push Tests: An Assesment of Bullet Engraving Forces in Varying Rffling Designs”, New Jersey, 2005.

[23] Heiney, O.K., “Ballistics Applied to Rapid Fire Guns”, Interior Ballistics of Guns, Progress in Astronautics and Aeronautics, Volume 66, New York, USA, 1979.

[24] Stals, J., “Form Functions for Multi-Component Propellant Charges İncluding Inhibited Grains and Sliver Burn”, Australian Defence Scientific Service, MRL-TN-371, 1975.

[25] Laney, C.B., “Computational Gasdynamics”, Cambridge University Press, 1998.

[26] Toro, E.F., “Approximate Riemann Solvers, Parameter Vectors and Difference Schemes”, Journal of Computational Physics, 1981.

[27] Toro, E.F., “A Fast Riemann Solver with Constant Covolume Applied to Random Choice Method”, International Journal for Numerical Methods In Fluids, Volume 9, 1989.